

Impurity peaking of SPARC H-modes: a sensitivity study on physics and engineering assumptions.

M. Muraca¹, P. Rodriguez-Fernandez¹, J. Hall¹, N.T. Howard¹,
D. Fajardo², G. Tardini², C. F. B. Zimmermann³, T. Body⁴

¹MIT Plasma Science and Fusion Center, 167 Albany St, Cambridge, MA 02139, USA

²Max Planck Institute for Plasma Physics, Boltzmannstrasse 2, Garching bei München, 85748, Germany

³Department of Applied Physics and Applied Mathematics, Columbia University, New York 10027, USA

⁴Commonwealth Fusion Systems, 117 Hospital Rd, Devens, MA 01434, USA

E-mail: mmuraca@mit.edu

December 2025

Abstract. In this paper, an overview of the impurity transport for three H-mode plasmas in the upcoming SPARC tokamak has been provided. The simulations have been performed within the ASTRA+STRAHL framework, using FACIT and TGLF-SAT2 to predict, respectively, neoclassical and turbulent core transport, while a neural network trained on EPED simulations has been employed to calculate the pedestal height and width self-consistently. A benchmark with previous simulations at constant impurity fraction has been provided for three H-modes, spanning different plasma current and magnetic field values. For a scenario, additional simulations have been performed to account for uncertainties in the modeling assumptions. The predictions are nearly insensitive to changes in the top of pedestal W concentrations. Varying the Ar pedestal concentration has shown a small effect on the impurity peaking and nearly constant fusion gain values, due to multiple effects on pedestal pressure, main ion dilution and density peaking. The inclusion of rotation in ASTRA simulations has shown minimal impact on confinement and impurity transport predictions. An exploratory study has been provided with a first set of simulations treating D and T separately, experiencing a maximum fusion power at 55-45% DT fuel composition, and an asymmetric distribution with respect to the D concentration. All the results, including sensitivity scans of toroidal velocity and ion temperature and density gradients, highlighted that turbulent impurity transport prevails on the neoclassical component, aligning with previous ITER predictions, and suggesting that next generation devices like SPARC, operating at low collisionality, will experience low W accumulation.

1. Introduction

The prediction of transport and confinement is crucial to determine the fusion performance of next generation devices, like ITER [51], DEMO [35], SPARC [15]

and ARC [78, 49]. Such a task can be performed with different strategies which vary depending on the precision and the computational time required by the models employed. Typically, models which can be run in real-time but have a limited amount of physics ingredients are referred to as *low-fidelity*. Examples are scaling laws [84] or data-driven models [54, 34], which are derived from experimental observations on existing machines, fitting procedures and statistical regressions. While such models are very useful to identify general trends and scope the design of future devices, their use for quantitative predictions should be approached with caution. On the other hand, *high-fidelity* simulations are usually conducted with non-linear gyrokinetic (GK) codes [41, 60, 47, 12, 31], which are capable of reproducing the physics accurately, but they remain computationally expensive, requiring up to several months to converge. These models are crucial to identify interesting physics and explore sophisticated effects like multi-scale turbulent interactions and saturation mechanisms, but their usage is limited by existing computational resources, and they can not be used to obtain extensive databases. The *medium-fidelity* simulations represent a good compromise between good predictive capability and low computational expenses. Example of medium-fidelity approaches are quasi-linear transport models like TGLF [82, 83] and QualiKiZ [9], whose fluxes can be found through a linear eigenvalue solver and a saturation rule previously fitted on non-linear GK simulations. These models typically require up to a few minutes to run.

Generally, transport models can be run at specific radial locations to investigate the dominant instability, or in an integrated way, connecting a series of radial points from the magnetic axis to the separatrix. The second approach, called "integrated modeling", evolves self-consistently the power and kinetic profiles, allowing to predict the fusion performance and confinement of future machines. Examples of integrated modeling codes are ASTRA [61, 62], TRANSP [58] or JINTRAC [72]. These codes are also referred to as flux-matching transport solvers, since they evolve two fluxes terms (the transported flux and the algebraic sum of sources and sinks) until they converge to the steady-state profiles.

The integrated transport modeling has been historically mainly conducted with medium fidelity models, but recent progress has opened up the possibility to employ non-linear GK models [17, 66, 68, 32]. Within the integrated modeling framework several assumptions can be made on the uncertain parameters, without including a detailed model to predict them. This allows to speed up the simulations and generate extensive databases. Examples of uncertain parameters assumed in the simulations are the H-mode pedestal density, fuel mix concentration or impurity radial profiles. It has been demonstrated in [56] that such parameters can dramatically impact the fusion gain and power. In particular the W concentration has been found to be a crucial parameter which governs the radiation and the H-mode accessibility. This has motivated a study of the impurity transport in the core, which was previously prescribed through fixed concentrations, as in the SPARC Physics Basis [15] and followup work. Such modeling aims at validating previous methodologies employed to quantify the variations

of performance, and explore the physics governing the impurity peaking in the core. Therefore, in this paper we predicted the impurity transport for 3 SPARC H-mode scenarios that are being considered for operation, covering different plasma current and magnetic field values. Scans of input power and pedestal density have been performed to study the robustness of the results. A previously unexplored H-mode scenario has been selected to perform additional scans of the boundary conditions for Ar and W concentrations, rotation and DT fuel mix composition. These sensitivity studies accounted for uncertainties on input parameters, showing minimal deviations of impurity peaking and fusion gain.

The remainder of the paper is organized as follows: in section 2, the framework of the simulations is described; in section 3, the SPARC H-mode scenarios are introduced and the nominal simulation results are shown, including a benchmark with previous results; in section 4 the Ar and W concentrations at the pedestal top are varied and the results are discussed; in section 5 the impact of rotation on impurity transport is explored; in section 6 a variation of DT fuel mix composition is performed and the results are analyzed; in section 7, the article is summarized and the conclusions are discussed, including an outlook for future work.

2. Simulation Setup

In order to predict the performance of a discharge, a series of models needs to be integrated in a framework which predicts plasma kinetic profiles. In the present paper, this task has been performed with the time-dependent transport solver ASTRA [61]. Although ASTRA can simulate the time trajectories of a plasma pulse, here we focused on the stationary flat-top phase of three H-mode scenarios, where equilibrium, kinetic profiles and fusion power have reached a converged state. The plasma equilibrium has been calculated with SPIDER [39], which performs fixed-boundary computations. The last closed flux surface (LCFS) coordinates are obtained with FreeGS [28] simulations. Both SPIDER and FreeGS solve the Grad-Shafranov equation [30, 75].

Core turbulent transport in modern, high-power tokamaks is driven by micro-instabilities like Electron Temperature Gradient (ETG), Trapped Electron Mode (TEM) and Ion Temperature Gradient (ITG) [88, 18, 29]. Here, turbulent transport in the core is predicted using the quasi-linear TGLF model [83]. TGLF is a common tool used in reactor design studies, which has been widely validated on different machines and plasma scenarios, showing reliability [70, 69, 4, 5, 16, 81]. The control settings adopted in this project include electromagnetic effects (δA_{\parallel}), five plasma species, Miller geometry [80], saturation rule SAT2 [83] and a maximum of 6 parallel basis functions.

The neoclassical impurity transport has been calculated with FACIT [22, 23], an analytical model which includes the effect of rotation and poloidal asymmetries, providing flux-surface averaged coefficients for arbitrary values of collisionality, charge, mass and radial position in the confined region. The atomic processes of impurities (e.g. ionization and recombination) are calculated self-consistently in STRAHL [19], which is called

within ASTRA at every computation time step. STRAHL calculates also the radiated power and transport of impurities for every charge state, taking as input the wall source, diffusivity (D) and convection (v) for every impurity involved in the simulations. While FACIT can provide D and v separately, TGLF calculates directly the combined particle flux. Therefore, in order to separate D and v , TGLF is called 2 times at every time step, once with a different impurity density gradient and once with the actual density profile, similarly as in [25]. This allows to separate the convective from the diffusive term, under the assumption of impurities being trace species, which do not impact the background turbulence.

The plasmas considered in this study are H-modes, therefore the pedestal stability must be evaluated in the context of peeling-ballooning theory. It is worth to mention that ELMy H-mode regimes are operationally challenging because of their high power and particle fluxes on Plasma-Facing Components (PFCs). However, the evaluation of operational strategies to mitigate ELMs is beyond the scope of the paper, and we consider such regimes as upper performance limits. The prediction of pedestal pressure is done using a neural network (NN) trained on EPED simulations of SPARC [77], following a procedure similar to [55]. This model was already introduced in [56], where its details are described. This model self-consistently updates the pedestal height as plasma gradients and stored energy evolve, allowing to correctly capture the effect of global beta on the pedestal pressure. In this NN framework, the pedestal density is an input parameter, as it depends on fueling, neutral penetration, and edge physics, which are not modeled here. The turbulent transport of impurities in the edge is tuned to achieve target concentrations at the top of pedestal. This choice is imposed by the lack of robust models which can be employed in an integrated framework. This represents a lack of self-consistency, but the task of this paper is to quantify core impurity peaking. Therefore, in this context, the pedestal model should only provide reasonable pedestal boundary conditions, while the precise quantification of edge transport is beyond the scope of the present work and the capabilities of this framework. However, a sensitivity study of pedestal concentrations has been performed in the paper to account for these uncertainties.

SPARC auxiliary power will be provided by the Ion Cyclotron Resonance Heating (ICRH) [50]. Since there is no self-consistent model to reproduce the ICRH absorption profiles within ASTRA, simulations were conducted using TRANSP [57], coupled with TORIC [10] and FPPMOD [33], to model ICRF wave propagation and Fokker Planck collisions. This is consistent with the methodology adopted in [56], ensuring that any variation in the results can be attributed to different assumptions on the impurity modeling, while keeping the ICRH input power constant. The resulting ICRH deposition profiles are imported into ASTRA simulations. The ohmic power is $P_{OH} = \sigma E_z^2$, where σ is the plasma conductivity and E_z is the electric field in the toroidal direction. The collisional exchange is $P_{ex} = 0.00246 \Lambda n_e n_i Z^2 (T_e - T_i) (AT_e^{3/2})^{-1}$, where Λ is the Coloumb logarithm, n_e and n_i are the electron and ion densities, T_e and T_i are the electron and ion temperatures, Z and A are the charge and mass of the main ion species.

The fusion power is $P_{fus} = 5P_\alpha = 5 \cdot 5.632n_D n_T \sigma_{DT}$, with an f_{ion} which calculates the fraction of power exchanged with ions and electrons, calculated as in [7]. As previously mentioned, P_{rad} is computed self-consistently in STRAHL, considering Bremsstrahlung, synchrotron and impurity line radiations for every charge state. Given the uncertainties in the neutral source penetration, especially in the typically stiff pedestals of H-modes, and the lack of reliable pedestal transport models, a top of pedestal density is assumed as boundary condition, and no D or T core particle source has been used in the simulations.

SPARC's compact design and the consequently high fluxes require a careful management of PFCs loads, to mitigate technological damages. Detachment, which represents a possible strategy to protect the divertor [43, 79, 48], is often achieved by injecting impurities into the Scrape-Off Layer (SOL), e.g. Ar, Ne or N. A small fraction of such impurities penetrates into the confined region, affecting the performance via radiation and dilution of the main ions. The presence of W, introduced by the erosion of PFCs, as well as plasma minority ions, used to efficiently heat the plasma with ICRH [86], further influences the core confinement. Therefore, in this paper, W, Ar and He3/H transport has been simultaneously modeled to quantify the impurity density peakings and their impact on performance. It is worth to mention that He3/H minorities are treated as thermal species, since a self-consistent Fokker-Planck collisional model is missing in ASTRA. This assumption is not valid near-axis, where most of the wave is absorbed, but in this work we are not addressing the effect of fast ions on turbulence, and the modeling of minority species aims at providing a realistic DT dilution and quantifying the He3/H core penetration to determine whether sufficient near-axis concentrations are reached to efficiently absorb ICRH power.

Sawteeth are expected to modify the safety factor and kinetic profiles in SPARC plasmas, particularly due to the absence of neutral beams, which could modify the q profile through current drive [71]. Although this study is not focused on magnetohydrodynamics (MHD), reliably calculating the safety factor profile is essential, since it directly affects transport. Therefore, the Kadomtsev model [42] has been used within ASTRA to predict the sawtooth inversion radius and flatten the safety factor profile. Additionally, ASTRA requires the sawtooth period as an input to trigger the profile relaxation. This period has been calculated with the Porcelli model [63] in TRANSP simulations for the 3 different analyzed scenarios, and it has subsequently been used as fixed parameter in ASTRA. A sensitivity study of the sawtooth period has been performed in [56], revealing a weak effect on the fusion power, which is calculated right before the sawtooth crash.

3. Benchmark of impurity transport simulations

In this section we discuss the results of our impurity modeling for three SPARC H-modes, and we compare them with simulations performed assuming fixed radial concentrations. The H-modes analyzed are the Primary Reference Discharge (PRD), the Reduced

Magnetic Field scenario (H8 or 8T), and the Reduced Plasma Current scenario (H12). The first two H-modes were already introduced in [56], while the third one was analyzed for the first time in this paper. These pulses are described separately in the remainder of the section.

3.1. Primary Reference Discharge

The PRD is a scenario envisioned in SPARC to maximize the reachable fusion gain. The main parameters are listed in table 1. This scenario adopts He3 minority species

Table 1: List of the main global and engineering parameters of the SPARC Primary Reference Discharge. Their definition is in [15].

Parameter	Value
B_t	12.2 T
I_p	8.7 MA
R_0	1.85 m
a	0.57 m
k_{sep}	1.97
δ_{sep}	0.54
P_{ICRH}	11 MW
$\langle n_e \rangle$	$3.1 \cdot 10^{20} m^{-3}$
q_{Uckan}^*	3.05
f_G	0.37
Z_{eff}	1.5

for efficient ICRH heating. As previously described, W, Ar and He3 sources and edge transport coefficients are artificially set to match top of pedestal target values of f_W , f_{He3} and Z_{eff} from previous modeling of the same discharge [56]. The same tuning approach has been used for the other scenarios analyzed in this paper. Therefore, given the arbitrariness behind the choice of edge transport and source, we will mainly refer directly to the resulting pedestal concentrations in the remainder of the paper. This choice reflects the scope of the present work, which does not attempt to determine limits on the impurity source originating from the scrape-off layer (SOL), but rather quantifying the core impurity peaking.

Simulations with and without impurity transport have been conducted, and the resulting fusion gain and $f_{LH} = P_{sep}/P_{LH}$ values, where P_{sep} and P_{LH} are respectively the power at the separatrix and the LH transition power threshold according to the Schmidtmayr scaling [74], are plotted in figure 1. Here, the squares are simulations with impurity transport, while the crosses are simulated assuming fixed concentrations. Red and green symbols refer respectively to the density and ICRH power scans. The results show a very good benchmark with almost no deviation, validating the simplified approach of

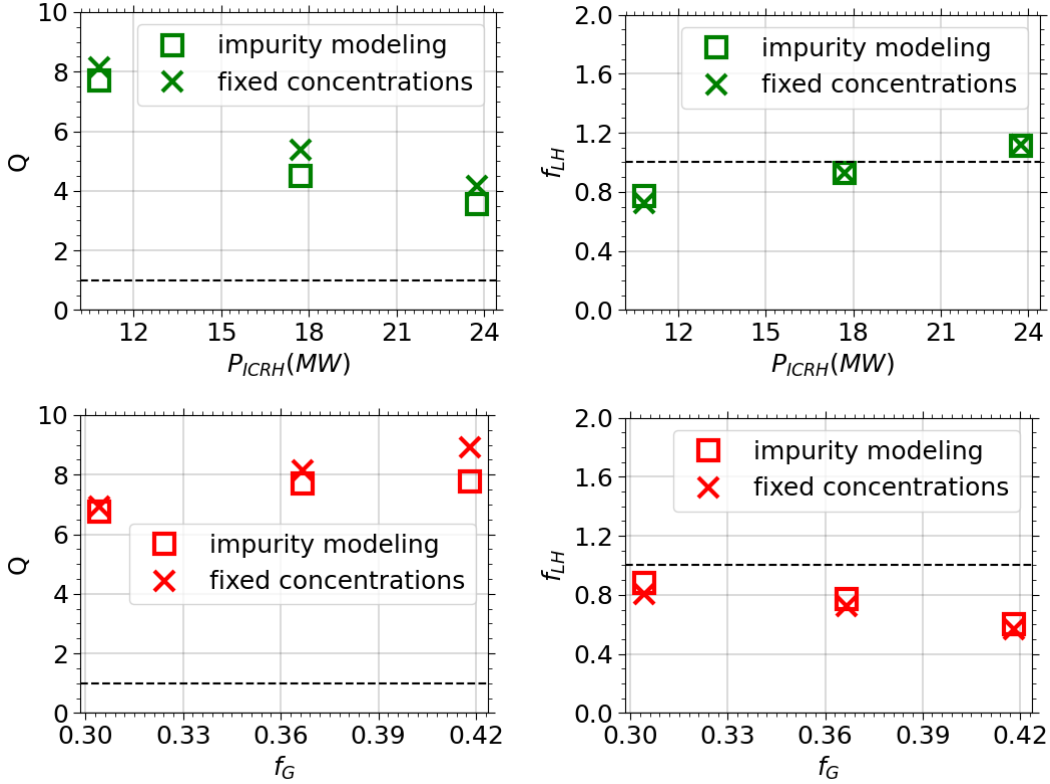


Figure 1: On the left and right are shown respectively fusion gain and f_{LH} values for an ICRH power (top plots, green) and density (bottom plots, red) scan of the PRD scenario. The squares indicate simulations with impurity transport, while the crosses are simulated keeping fixed radial impurity concentrations.

assuming fixed flat concentrations. The core impurity peaking is dominated by the turbulence, while the neoclassical contribution is negligible in these conditions. Such finding is consistent with [26], and is justified by high ion temperature gradient and low rotation conditions, which typically exhibit a small neoclassical pinch [1, 13, 23]. The neoclassical and turbulent W convections and diffusivities are compared in figure 2, showing that D and V are both dominated by the turbulence. The same result has been found for Ar, showing respectively a 3% and 4% maximum contribution of neoclassical diffusivity and convection. In the same figure, f_W , f_{He3} and Z_{eff} are also shown for the simulations with fixed and evolving impurity densities, indicating that a 4% He3 on-axis concentration can be reached with a 5% value at top of pedestal. In figure 2 the solid or dashed lines indicate the mean profiles, while the shaded areas around them show the maximum and minimum values obtained across all the simulations. The same style will be used to show profiles variations in the remainder of the article.

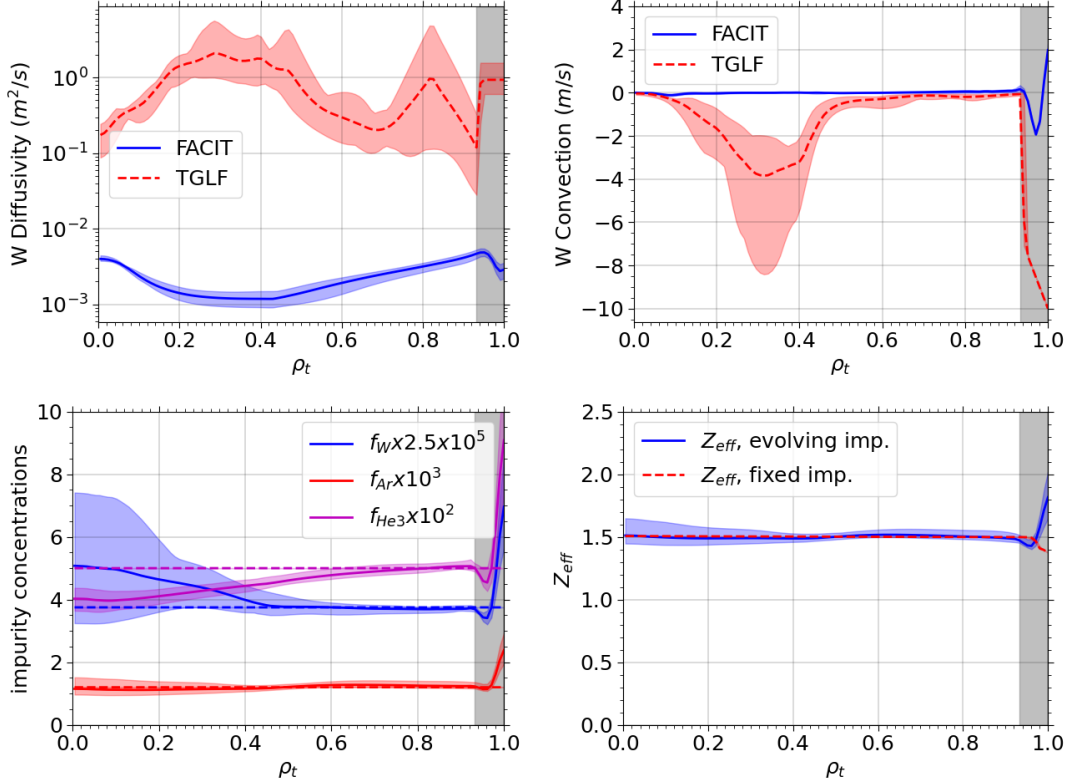


Figure 2: PRD profiles. Top left: turbulent (red) and neoclassical (blue) W diffusivity; top right: turbulent (red) and neoclassical (blue) W convection; bottom left: impurity concentrations; bottom right: Z_{eff} . In the bottom plots, the dashed lines indicate the simulations with fixed concentrations. The colored shades indicate the maximum and minimum values computed across the scans. The gray area is from top of pedestal to the separatrix.

3.2. Reduced Magnetic Field, $I_p = 5.7$ MA

The low magnetic field H-mode (H8) is a scenario considered for SPARC early operation. Its main parameters are listed in table 2. This H-mode operates at a lower $B_t = 8$ T

Table 2: List of the main engineering parameters of the SPARC 8T H-mode discharge. Their definition is in [15].

Parameter	Value
B_t	8 T
I_p	5.7 MA
k_{sep}	2
δ_{sep}	0.54
q_{Uckan}^*	3
Z_{eff}	1.5

constrained by the ICRH heating technique at 120 MHz based on near-axis power absorption of a H minority species. To maintain the same q^* , the plasma current has been reduced. Such variations of global parameters are expected to reflect lower performance than the PRD, making this scenario more suitable for the early operation of SPARC. For this pulse a density scan has been performed, following the same methodology used for the PRD, and assuming $P_{ICRH} = 25MW$. The results of the scan are shown in figure 3. This figure shows an almost perfect match of fusion gain, validating the simplified

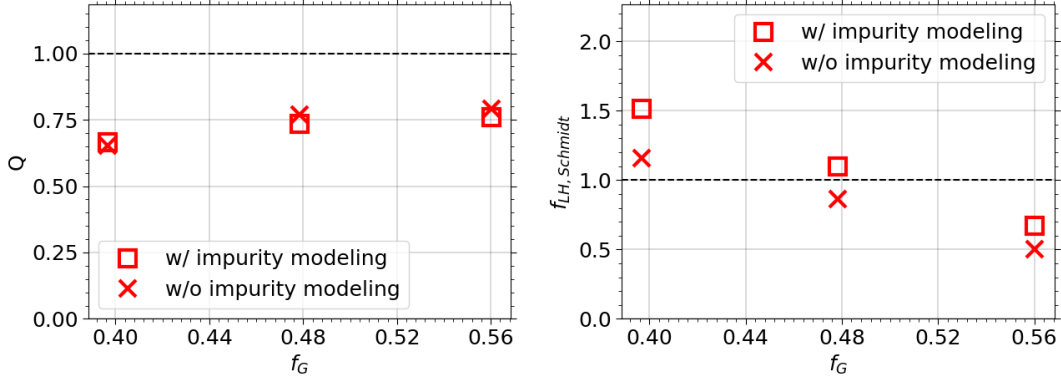


Figure 3: On the left and right are shown respectively fusion gain and f_{LH} values for a density scan of the 8T H-mode scenario, with $P_{ICRH} = 25MW$. The squares indicate simulations with impurity transport, while the crosses are simulated keeping fixed radial impurity concentrations.

approach with fixed impurity concentrations. f_{LH} shows instead an offset between the two simulation approaches. In particular, the cases with impurity transport are more optimistic about H-mode accessibility. The reason behind the mismatch is the difference in the predicted ion heat flux, which affects f_{LH} , using the Schmidtmayr scaling. The different Q_i is caused by the different radiation calculated in the simulations. In fact, in figure 4, one can see that most of the power fluxes are similar using STRAHL or fixing the impurity concentrations, but a deviation of the radiative power causes a lower electron temperature which is reflected in a smaller collisional exchange from electrons to ions. The temperature profiles for the case at lowest density are shown in figure 5. The lower collisional exchange causes lower Q_i in the simulations with fixed concentrations. In order to verify the origin of the mismatch in the radiative power, P_{rad} from Bremsstrahlung, W and Ar has been plotted in figure 6. The figure shows a great match for W and a small deviation for Ar, while the biggest discrepancy is found for the Bremsstrahlung radiation. In the simulations without STRAHL, $P_{rad,W}$ and $P_{rad,Ar}$ are calculated respectively as in [65] and [64], while $P_{Bremsstrahlung} = 5.06 \times 10^{-5} Z_{eff} n_e^2 \sqrt{T_e}$, as in [85]. The maximum $P_{Bremsstrahlung}$ deviation is 33%, which is reflected also in $f_{LH,Schmidtmayr}$ in figure 3, showing that the simplified formula used in the simulations with fixed concentration can overestimate the radiative power. For comparison, the H-mode robustness calculated with the Martin scaling [52] has been analyzed as well.

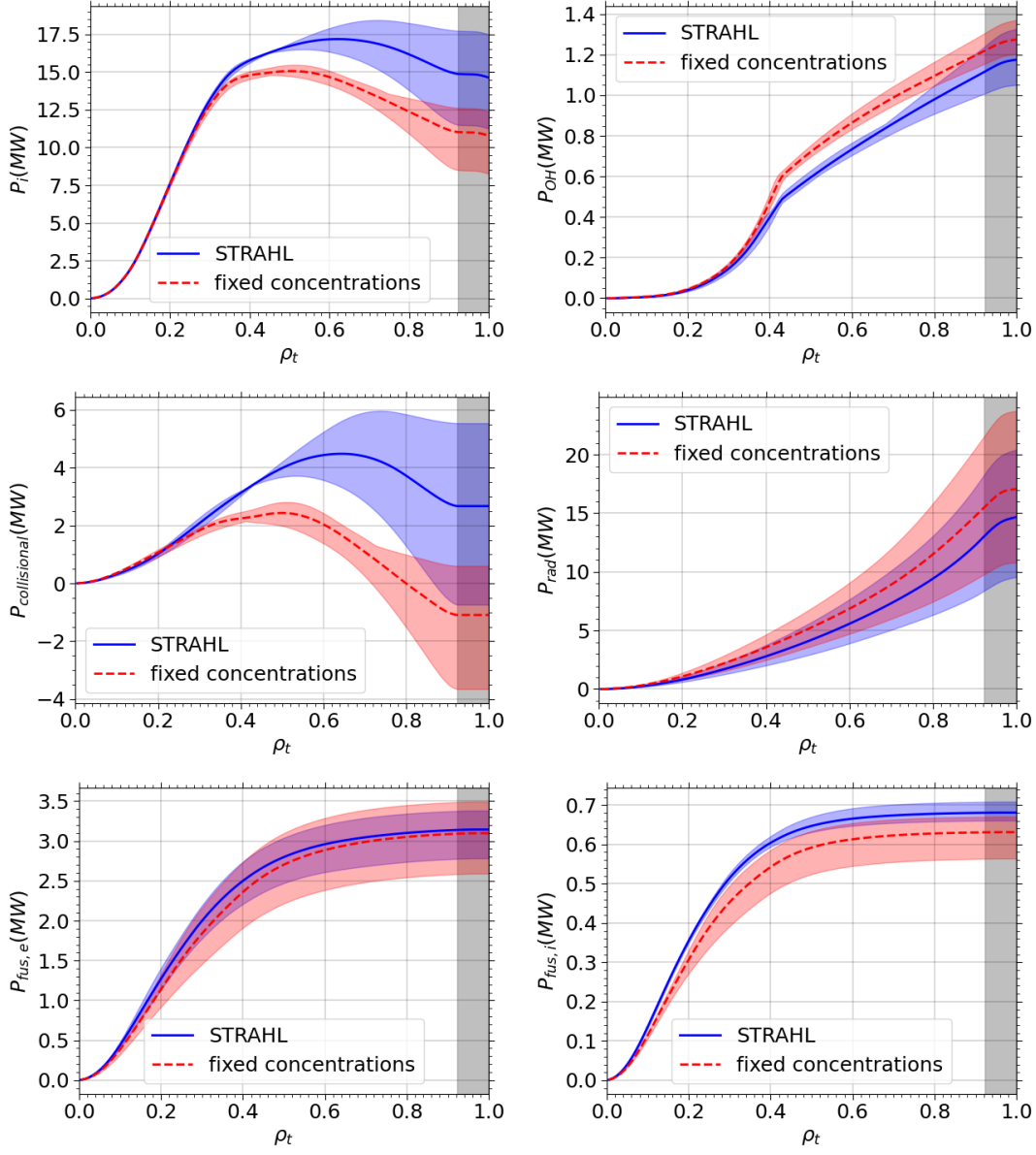


Figure 4: Integrated radial profiles of the power fluxes for a density scan of the SPARC H8 scenario, using STRAHL (blue) and fixed impurity concentrations (red). Top left: total ion power; top right: ohmic power; center left: collisional exchange; center right: radiative power; bottom left: fusion power to electrons; bottom right: fusion power to ions. The solid/dashed lines indicate the nominal simulations, while the shaded area show the maximum and minimum values of the profiles across the density scan. The gray region indicates from top of pedestal to the separatrix.

Table 3 compares $f_{LH,STRAHL}/f_{LH,fixed}$ using Martin and Schmidtmayr scalings, where $f_{LH,STRAHL}$ is calculated in the simulations with STRAHL, and $f_{LH,fixed}$ in the cases with fixed impurity concentrations. The table shows higher f_{LH} values in STRAHL simulations with both scalings. However, while $(f_{LH,STRAHL}/f_{LH,fixed})_{Schmidtmayr}$ is

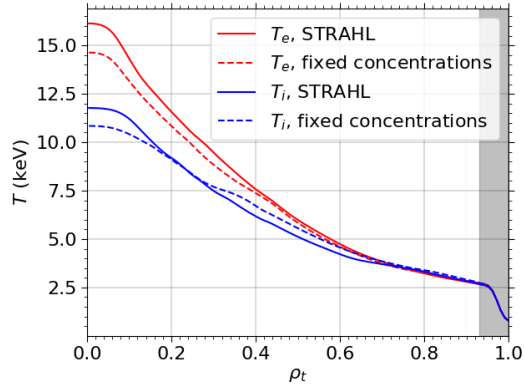


Figure 5: Temperature profiles at the lowest density of the SPARC H8 scenario, using STRAHL (solid) and fixed impurity concentrations (dashed). Red (blue) indicates the electron (ion) temperature. The gray region indicates from top of pedestal to the separatrix.

Table 3: $f_{LH,STRAHL}/f_{LH,fixed}$ for different Greenwald fractions, using Martin or Schmidtmayr scaling.

f_G	$(f_{LH,STRAHL}/f_{LH,fixed})_{Martin}$	$(f_{LH,STRAHL}/f_{LH,fixed})_{Schmidtmayr}$
0.39	1.06	1.3
0.48	1.2	1.27
0.56	1.5	1.33

constant across the scan, $(f_{LH,STRAHL}/f_{LH,fixed})_{Martin}$ increases with density, showing high discrepancy at maximum f_G . The reason behind this behavior is the crucial role that radiation plays in the electron heat flux, which is included in the $f_{LH,Martin}$ computation. In fact, when using the Martin scaling, Q_e is directly affected by P_{rad} , while Q_i and $f_{LH,Schmidtmayr}$ are influenced only indirectly through modifications of the electron temperature and collisional exchange. The discrepancy in f_{LH} was not observed for the PRD, because for such scenario the fusion power is significantly higher, making the radiation and collisional exchange contributions small at the W concentrations predicted in the simulations. The neoclassical pinch and turbulent diffusivity of the simulations are shown in figure 7, together with the impurity concentrations. As found for the PRD, the W and Ar turbulent transport prevails on the neoclassical one and the impurity concentrations are mostly flat, matching the simplified simulations.

3.3. Reduced Plasma Current, $B_t = 12 T$

In an attempt to identify non-L-mode scenarios that reach breakeven conditions, we have investigated an additional H-mode operated with 12 T and reduced plasma current. Such pulse has been found through a scoping of the operational space, exploring different values of the engineering and global parameters. An initial broad

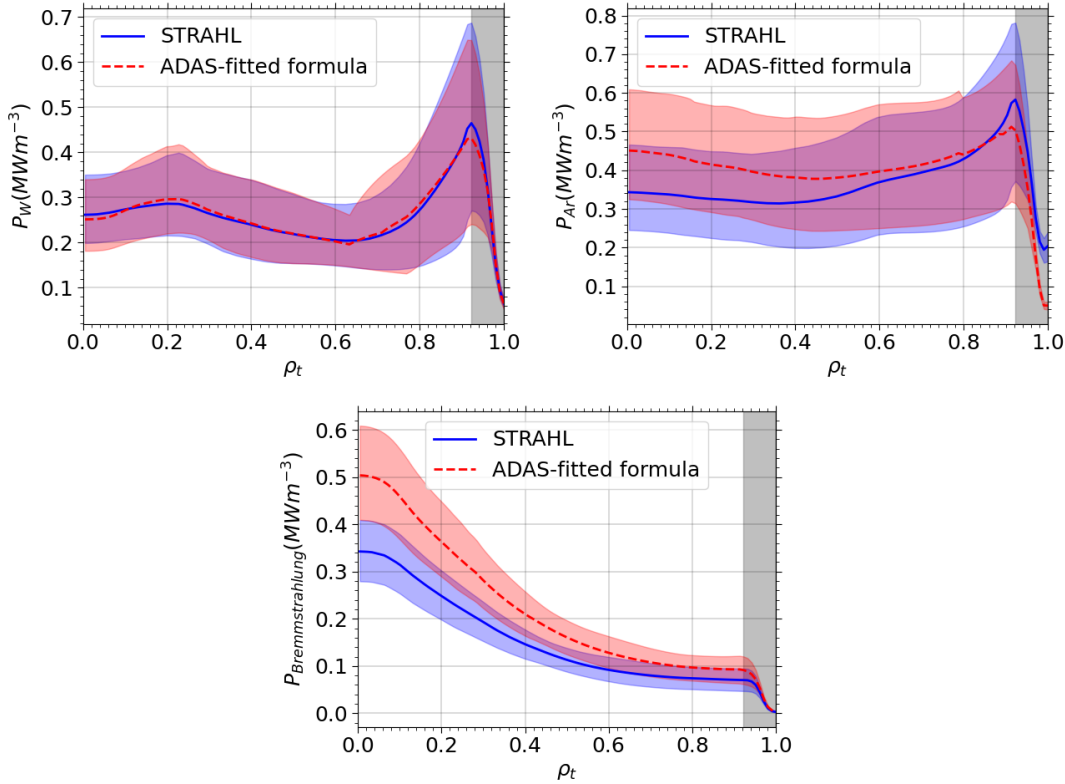


Figure 6: Radiative power density profiles for a density scan of the SPARC H8 scenario, using STRAHL (blue) and fixed impurity concentrations (red). Top left: W radiation; top right: Ar radiation; bottom: Bremsstrahlung radiation. The solid/dashed lines indicate the nominal simulations, while the shaded area show the maximum and minimum values of the profiles across the density scan. The gray region indicates from top of pedestal to the separatrix.

scope has been performed with Plasma OPERational CONtour (POPCON) [36], which couples 0D models (e.g. scaling laws), functional forms to describe kinetic profiles, and physical/technological constraints (e.g. q^* or q_{95}) to find scenarios which meet certain requirements, as a specific fusion gain or power. This has been done with the additional constraint of $f_{LH} > 1$ (i.e. accessing H-mode according to both Martin and Schmidtmayr scalings). The results produced the global parameters listed in table 4. It is worth to notice the higher Z_{eff} compared to the previously analyzed H-modes. Such estimate is reflected by a heavy SOL Ar seeding aimed at protecting the divertor and PFCs at the high q_{95} conditions reached here. After the initial POPCON exploration, an additional scoping has been performed with ASTRA, using fixed impurity concentrations, and performing a 4D scan of density at top of pedestal, ICRH input power, W concentration and plasma current. The ranges of variation of such parameters are listed in table 5. With these permutations a total amount of 657 simulations was obtained, largely spanning the operational space. As found in [56] for the PRD and the 8T H-modes, the conditions which maximize core fusion gain and

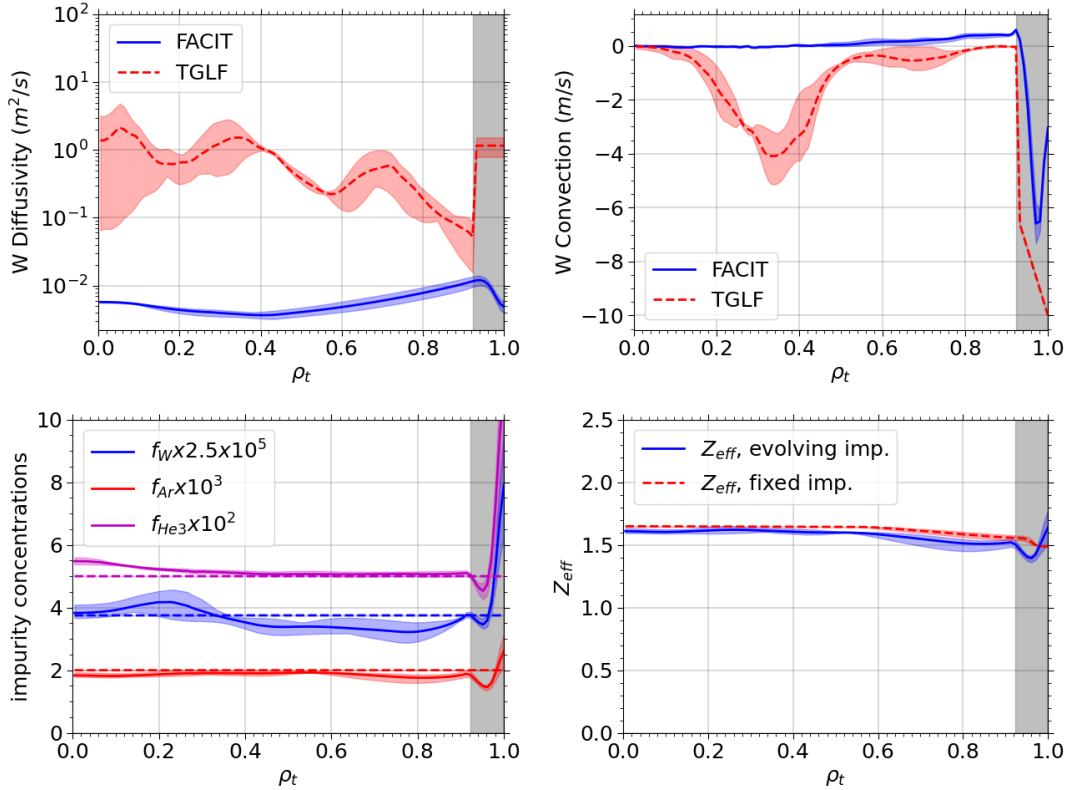


Figure 7: 8T H-mode profiles. Top left: turbulent (red) and neoclassical (blue) W diffusivity; top right: turbulent (red) and neoclassical (blue) W convection; bottom left: impurity concentrations; bottom right: Z_{eff} . In the bottom plots, the dashed lines indicate the simulations with fixed concentrations. The colored shades indicate the maximum and minimum values computed across the scans. The gray region indicates from top of pedestal to the separatrix.

Table 4: List of the main engineering parameters of the reduced current H-mode discharge. Their definition is in [15].

Parameter	Value
B_t	12.2 T
I_p	6.5 MA
k_{sep}	2
δ_{sep}	0.48
q_{Uckan}^*	3.6
Z_{eff}	3.0

H-mode access probability are low density and high ICRH input power. The effect of such conditions on the exhaust and PFCs protection has not been investigated here. The results of this exploration are shown in figure 8, where the suitable operational

Table 5: Ranges of variation of engineering and global parameters for the reduced current H-mode.

Parameter	Value
I_p	[5.5 - 6.5] MA
P_{ICRH}	[15 - 25] MW
n_{top}	[1.8 - 3.3] $10^{20} m^{-3}$
f_W	[1.5 - 13.5] 10^{-5}

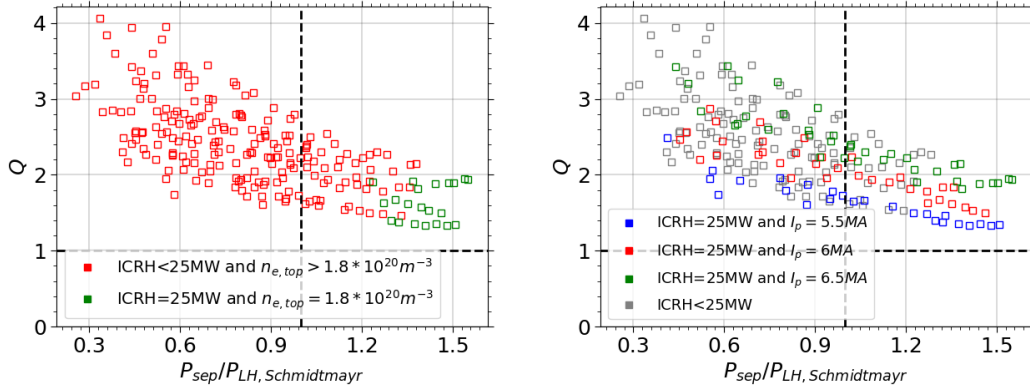


Figure 8: Left: Q vs f_{LH} for the H12 scenario. The green squares are simulations with maximum available P_{ICRH} and lowest top of pedestal density. Right: Q vs f_{LH} for maximum ICRH input power and different I_p values. Gray squares are simulations with $P_{ICRH} < 25 MW$, at any plasma current.

window for breakeven campaign is where $Q > 1$ and $f_{LH} > 1$. In the left plot, the green symbols indicate simulations at the lowest density and highest ICRH input power. In the right plot, an additional result is shown: the breakeven H-mode sustained condition can be reached at different levels of plasma current. This ensures a certain flexibility in the choice of q_{95} , allowing for multiple strategies to handle exhaust power. The scoping of the operational space performed with ASTRA has identified ideal values of density and ICRH power at a certain prescribed W concentration. The results should then be compared with higher-fidelity simulations which include impurity transport, as the ones previously performed for PRD and H8. The results of such comparison are shown in figure 9, showing a top of pedestal and ICRH power scan. For this scenario a very good benchmark has been obtained, with a small deviation of f_{LH} , similarly to H8. The turbulent diffusivity and neoclassical pinch are plotted in figure 10 for Ar and W, together with impurity concentrations and Z_{eff} . The figure shows that the W anomalous transport is considerably higher than the neoclassical pinch, and as a consequence the radial W concentration is roughly constant. However, He3 and Ar show slightly hollowed concentration profiles, showing that the assumption of fixed concentrations is conservative for radiation and f_{LH} calculations. The hollowed Ar

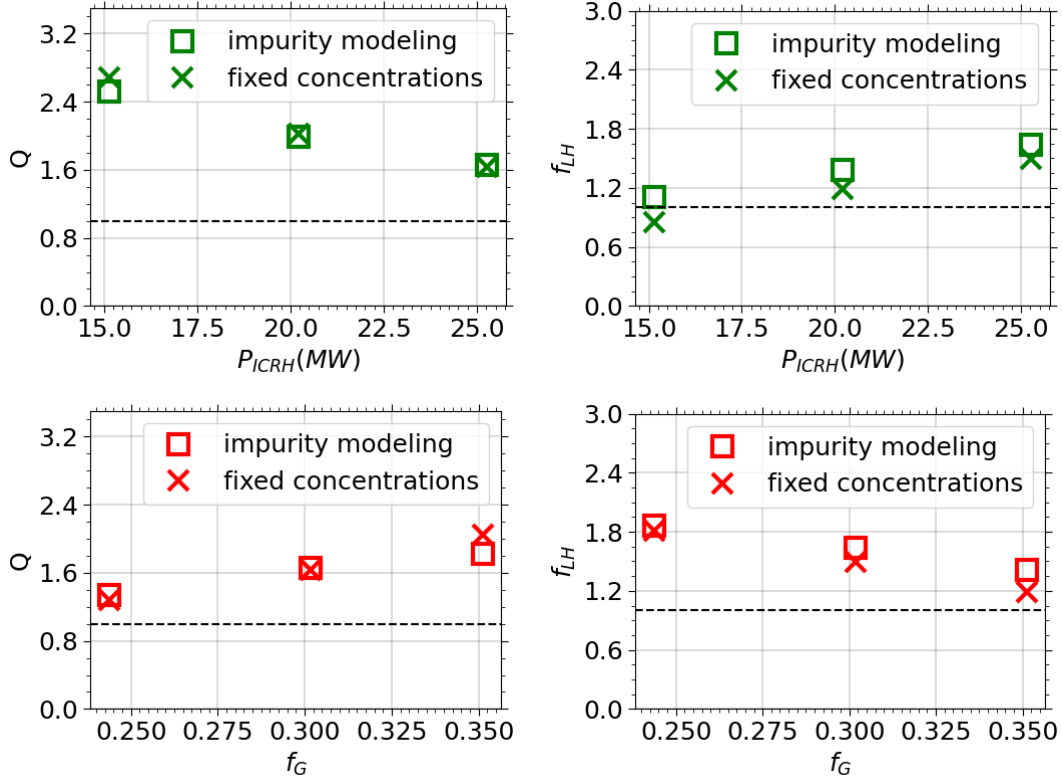


Figure 9: On the left and right are shown respectively fusion gain and f_{LH} values for an ICRH power (top plots, green) and density (bottom plots, red) scan of the H12 scenario. The squares indicate simulations with impurity transport, while the crosses are simulated keeping fixed radial impurity concentrations.

profile is reflected also by Z_{eff} , as shown in figure 10.

4. Sensitivity of impurity peaking to Ar and W pedestal concentrations

The simulations shown in this work assumed a set of boundary conditions for the impurity concentrations at the top of pedestal. This choice is justified by the difficulty of modeling turbulent transport in the edge of a H-mode. However, the concentrations at the pedestal position are uncertain. Therefore, for the H12 scenario, scans in Ar and W concentrations have been performed to study the impact on the impurity peaking, H-mode robustness and fusion performance. These concentrations have been obtained scanning the impurity sources from the wall in STRAHL and keeping a fixed turbulent impurity transport in the edge. The ranges of variation of the scans are listed in table 6. Increasing the W concentration, an effect on the H-mode sustainability has been found, as expected, due to the higher W radiation. However, a minimal impact has been observed on the fusion performance and impurity peaking. The impurity transport coefficients are plotted in figure 11 for all species. The kinetic profiles are plotted in figure 12, together with the impurity densities. One can notice that there is almost

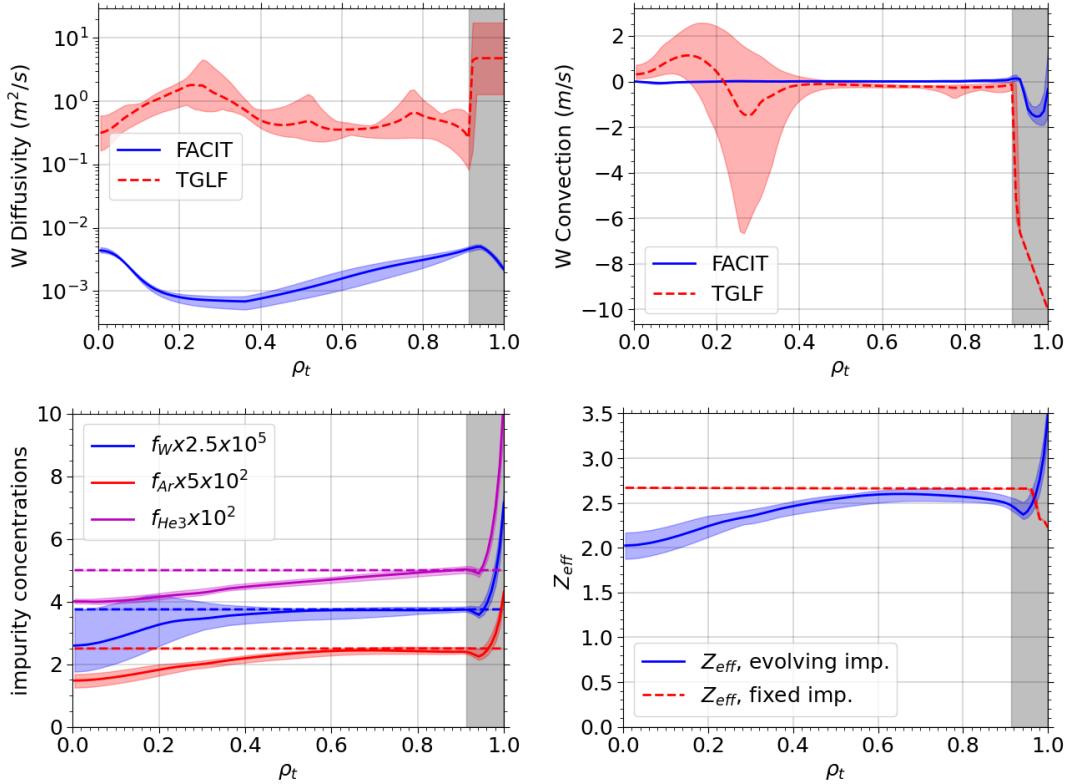


Figure 10: Low current H-mode profiles. Top left: turbulent (red) and neoclassical (blue) W diffusivity; top right: turbulent (red) and neoclassical (blue) W convection; bottom left: impurity concentrations; bottom right: Z_{eff} . In the bottom plots, the dashed lines indicate the simulations with fixed concentrations. The colored shades indicate the maximum and minimum values computed across the scans. The gray region indicates from top of pedestal to the separatrix.

Table 6: Ranges of variation of W and Ar top of pedestal concentrations for the H12 scenario.

Concentration	
W scan	$f_{W,top} = [0.6 - 6] \times 10^{-5}$
Ar scan	$f_{Ar,top} = [0.5 - 8] \times 10^{-3}$

no effect on the kinetic profiles. This is due to the stiffness of the kinetic profiles [38, 73] which characterizes the high power H-mode scenario analyzed here. The left plot of figure 14 shows a small deviation of the electron and ion heat fluxes, due to the different radiation contribution. On the right plot of the same figure, χ_i/χ_e is pictured, showing average values consistent with typically ITG-dominated regimes [46]. The Ar and He3 profiles show minimal variations, decreasing their average densities at higher W concentrations. Such variations are probably associated with the slightly higher

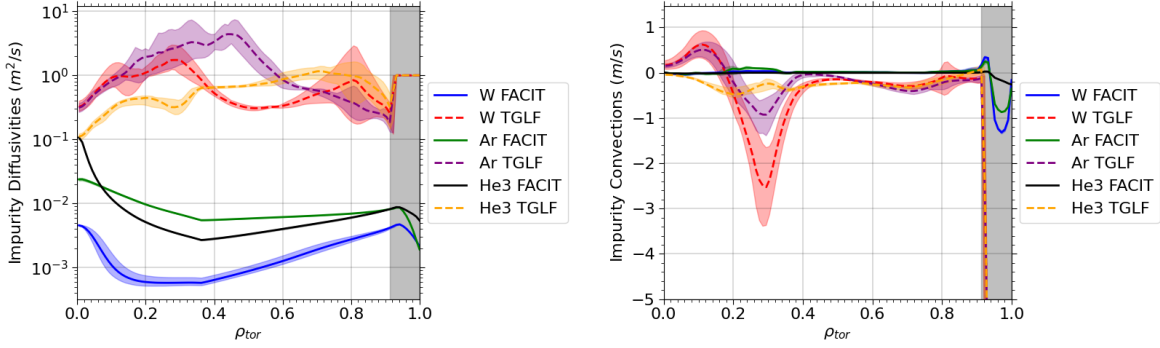


Figure 11: Scan of W pedestal concentration for the H12 scenario. Profiles of turbulent (dashed) and neoclassical (solid) transport coefficients. On the left (right) the diffusivities (convections) are shown for all the impurities. The colored shades indicate the maximum and minimum values computed for the transport coefficients across the scan. The gray area is from top of pedestal to the separatrix.

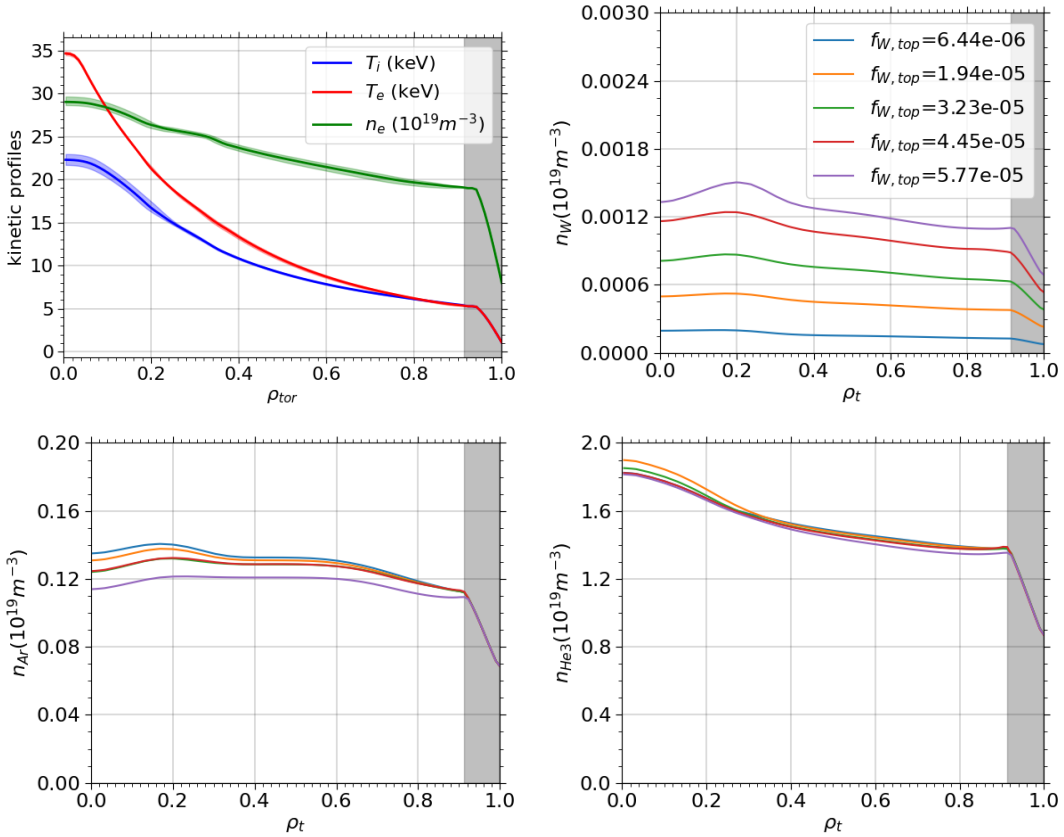


Figure 12: Profiles for a scan of W pedestal concentration in the H12 scenario. Top left: kinetic profiles; top right: W density; bottom left: Ar density; bottom right: He3 density. The colored shades (top left) indicate the maximum and minimum profiles computed across the scan. The gray area is from top of pedestal to the separatrix.

Z_{eff} reached at higher f_W values. However, since the f_W scan (larger than an order of magnitude) has produced a local maximum variation of 8% in the profiles, further investigation has not been considered necessary.

The scan in Ar concentration provided interesting results. The impurity transport coefficients are shown in figure 13, while the kinetic and impurity density profiles are shown in figure 15. Figure 11 and 13 confirm that the anomalous impurity transport

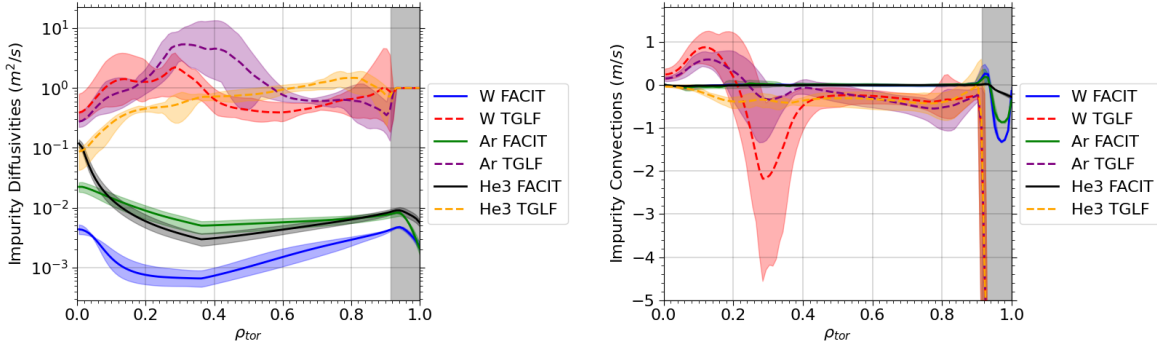


Figure 13: Scan of Ar pedestal concentration in the H12 scenario. Profiles of turbulent (dashed) and neoclassical (solid) transport coefficients. On the left (right) the diffusivities (convections) are shown for all the impurities. The colored shades indicate the maximum and minimum values computed for the transport coefficients across the scan. The gray area is from top of pedestal to the separatrix.

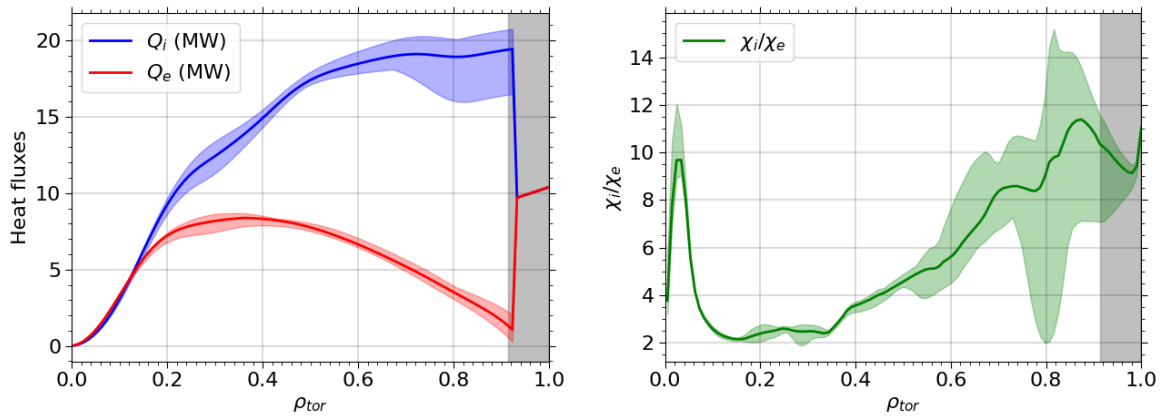


Figure 14: On the left the ion (blue) and electron (red) heat fluxes are shown, while on the right χ_i/χ_e is pictured. The colored shades indicate the maximum and minimum values computed across the W concentration scan. The gray area is from top of pedestal to the separatrix.

prevails on the neoclassical one in the core, as was previously found for all the performed simulations, including PRD and H8 scenarios. In figure 15, the kinetic profiles show a non-negligible variation across the Ar scan. In fact, a variation of Ar content affects multiple physics processes at the same time. In particular, a higher f_{Ar} :

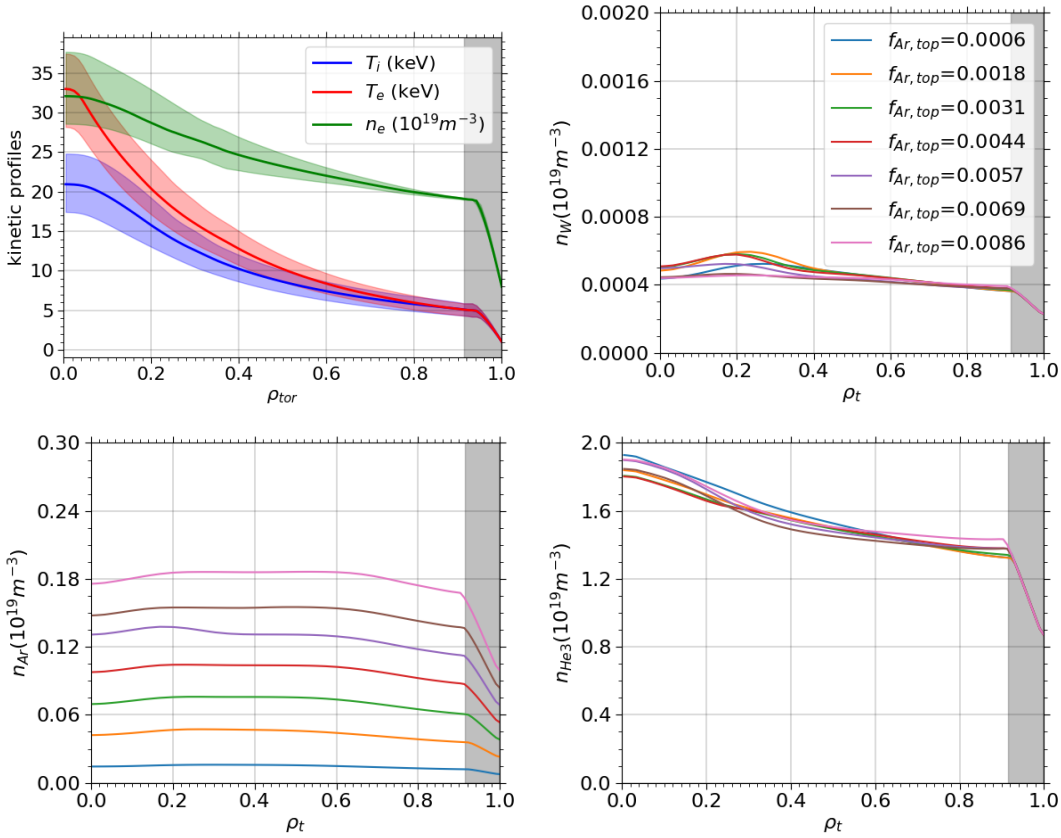


Figure 15: Profiles for a scan of Ar pedestal concentration in the H12 scenario. Top left: kinetic profiles; top right: W density; bottom left: Ar density; bottom right: He3 density. The colored shades (top left) indicate the maximum and minimum profiles across the scan. The gray area is from top of pedestal to the separatrix.

- leads to a higher Z_{eff} . This has a double effect: first, it impacts the ITG/TEM core instability balance. In fact, a higher Z_{eff} increases the ITG linear stability threshold [40], making the plasma more TEM-dominated, condition which typically shows a lower density peaking [21]; second, it increases the top of pedestal pressure (i.e. higher temperatures at fixed input density), since for the simulated electron density the pedestal stability is peeling-constrained;
- increases the main ion (DT) dilution, affecting turbulence [20, 44, 67] and leading to a smaller amount of fuel for fusion reactions;
- increases the radiative power, reducing the H-mode robustness.

All the effects discussed above can be observed in figure 16. While the higher radiation has a clear impact on H-mode sustainment, the overall effect on fusion performance is less trivial. In fact, the higher pedestal facilitates the production of higher fusion power, but the lower density peaking reduces P_{fus} and the lower DT concentration reduces the available fuel for fusion reactions. As a result of all the competing terms, the fusion power is roughly constant, as can be seen at the bottom right plot of figure 16. It

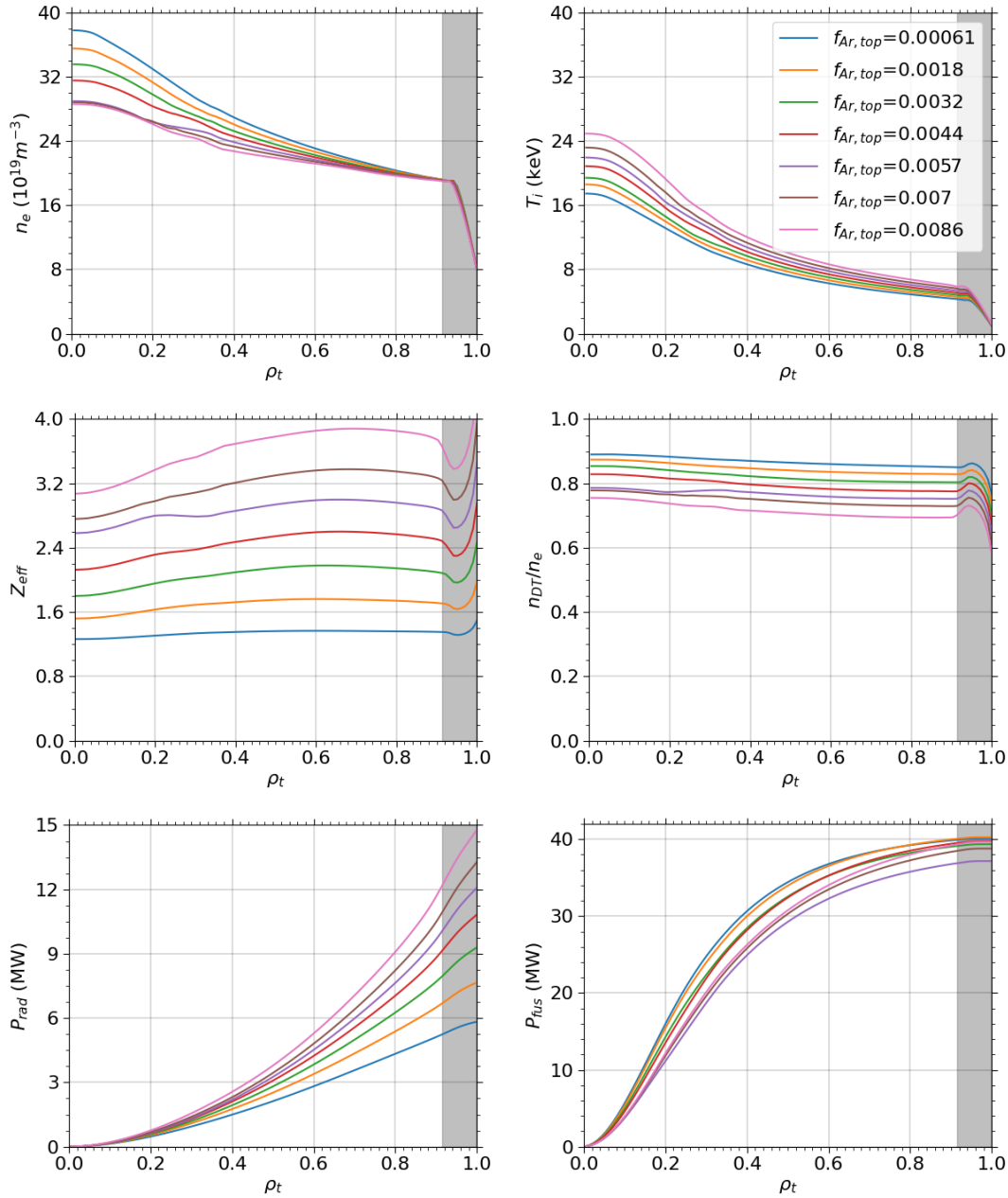


Figure 16: Profiles for a scan of Ar pedestal concentration in the H12 scenario. Top left: electron density; top right: ion temperature; center left: effective charge; center right: DT concentration; bottom left: cumulative radiative power; bottom right: total fusion power. The gray area is from top of pedestal to the separatrix.

is worth to mention that a similar competition between positive and negative effects has not been found across the W scan, since its low concentration makes it a trace species, not affecting considerably Z_{eff} and the DT dilution. A few global parameters to summarize the results of the W and Ar concentration scans are respectively listed in table 7 and 8.

Table 7: Global parameters for the scan in W pedestal concentration of the H12 scenario.

$f_{W,top} (10^{-5})$	$\langle T_i \rangle (keV)$	$P_{rad} (MW)$	Q	$f_{LH,Schmidt}$
0.6	8	10.7	1.43	1.58
2	8.05	12	1.43	1.57
3.3	8.1	13.5	1.45	1.55
4.6	8.18	15	1.45	1.51
6.	8.2	15.7	1.52	1.51

Table 8: Global parameters for the scan in Ar pedestal concentration of the H12 scenario.

$f_{Ar,top} (10^{-3})$	$\langle Z_{eff} \rangle$	$p_{top} (kPa)$	$\langle f_{DT} \rangle$	ν_{ne}	$P_{rad} (MW)$	Q	$f_{LH,Schmidt}$
0.5	1.34	256	0.87	1.66	5.8	1.54	1.61
1.8	1.7	272	0.85	1.59	7.7	1.55	1.6
3.2	2.1	290	0.82	1.53	9.3	1.51	1.59
4.6	2.5	304	0.79	1.47	10.8	1.53	1.59
6	2.9	320	0.77	1.37	12	1.43	1.57
7.2	3.3	337	0.75	1.38	13.3	1.49	1.57
8.6	3.8	358	0.72	1.38	14.8	1.52	1.56

5. Impact of rotation on impurity transport

The previously performed simulations assumed zero toroidal velocity. Although such an assumption is conservative in maximizing the turbulent transport [87, 45, 11, 6, 37], it is typically associated with low impurity accumulation [1, 23]. Therefore, the analytical model developed in [90] has been implemented in ASTRA to predict core toroidal rotation and its effect on neoclassical and turbulent transport, respectively through the Mach number and radial electric field. This model consists of a set of analytical expressions aimed at predicting the momentum diffusivity, convection and intrinsic torque. It has been validated on AUG and D3D discharges [89, 90]. It is worth to mention that the model does not treat the effect of ripples [27] and NTV torque [59, 14], which could lead to counter-current intrinsic torque in case of strong edge error fields. The description of such effects is beyond the scope of this paper. Simulations have been performed including momentum transport and using the analytical expressions up to the top of pedestal position. This choice is justified by the fact that the model was validated in the core. Therefore, a scan of flat toroidal rotation values from top of pedestal to the separatrix has been performed to account for uncertainties. This choice is supported by experimental evidence from Alcator C-Mod, which shows that the variation of the edge toroidal rotation in the absence of strong beam heating in an ICRH-dominated plasma is very limited and co-current [53]. The resulting impurity transport coefficients are shown in figure 17, while the kinetic and parallel velocity profiles are shown in

figure 18. The figures show respectively a small and no variation in the turbulent

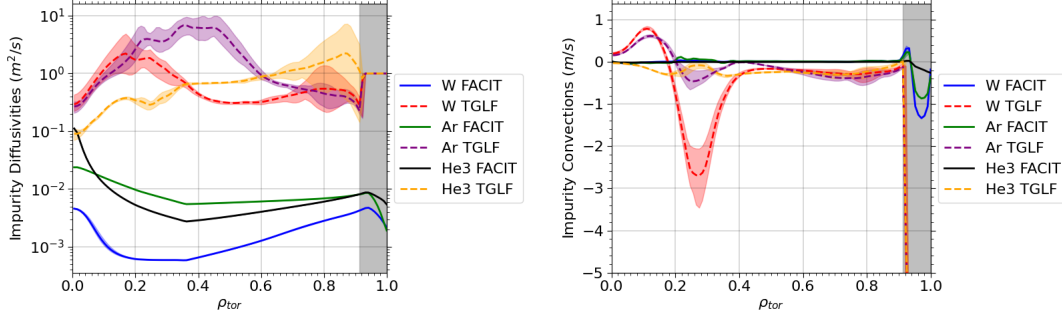


Figure 17: Scan in edge toroidal rotation for the H12 scenario. Profiles of turbulent (dashed) and neoclassical (solid) transport coefficients. On the left (right) the diffusivities (convections) are shown for all the impurities. The colored shades indicate the maximum and minimum values computed for the transport coefficients across the scan. The gray area is from top of pedestal to the separatrix.

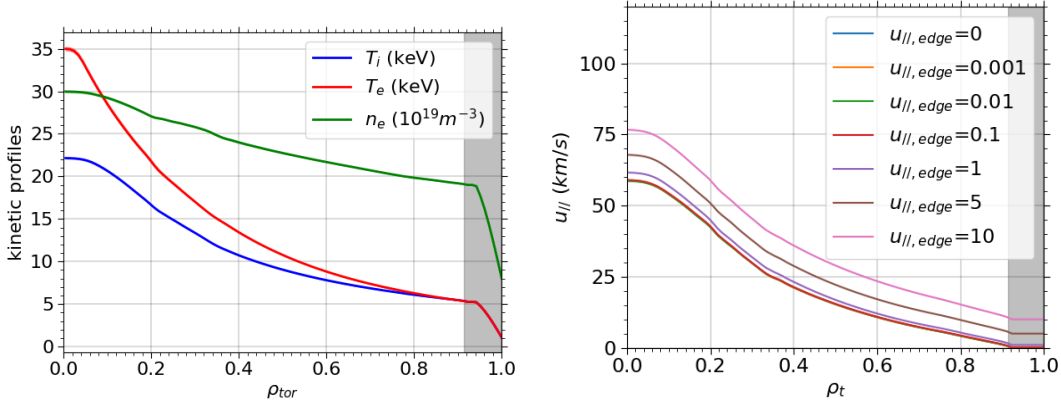


Figure 18: Kinetic (left) and parallel velocity (right) profiles for a scan in edge toroidal rotation of the H12 scenario. The colored shades indicate the maximum and minimum kinetic profiles computed across the scan. The gray area is from top of pedestal to the separatrix.

coefficients and kinetic profiles. Figure 17 highlights how the neoclassical transport is basically identical across the scan. This is justified by the low collisionality of the plasma, where the variation in rotation has a weak effect on neoclassical pinch and diffusivity [23]. This observation has motivated a deeper analysis into the neoclassical transport coefficients obtained by FACIT. In fact, a multi-dimensional scan of the main ion temperature and density gradients and of the toroidal rotation have been performed around the nominal H12 simulation. Such scan aims at finding the thresholds above which the neoclassical transport becomes comparable with the anomalous one. The ranges in which the parameters were varied are shown in table 9. It is worth mentioning

Table 9: Variation ranges of normalized n_i and T_i gradients and toroidal rotation for individual scans of FACIT standalone at $\rho_t = 0.25$. The scaling factors refer to a nominal ASTRA+TGLF+FACIT simulation.

scan parameter	scaling factors	values
v_{tor}	–	$[5 - 300] \times 10^4 [m/s]$
R/L_{T_i}	$[0.0025 - 1]$	$[0.0125 - 5]$
R/L_{n_i}	$[1 - 10]$	$[1.8 - 18]$

that the variation ranges of the scans have been intentionally chosen unrealistically wide as a numerical exercise to find the transition to neoclassically dominated impurity transport. The results of the scans are summarized in figure 19. This figure shows several

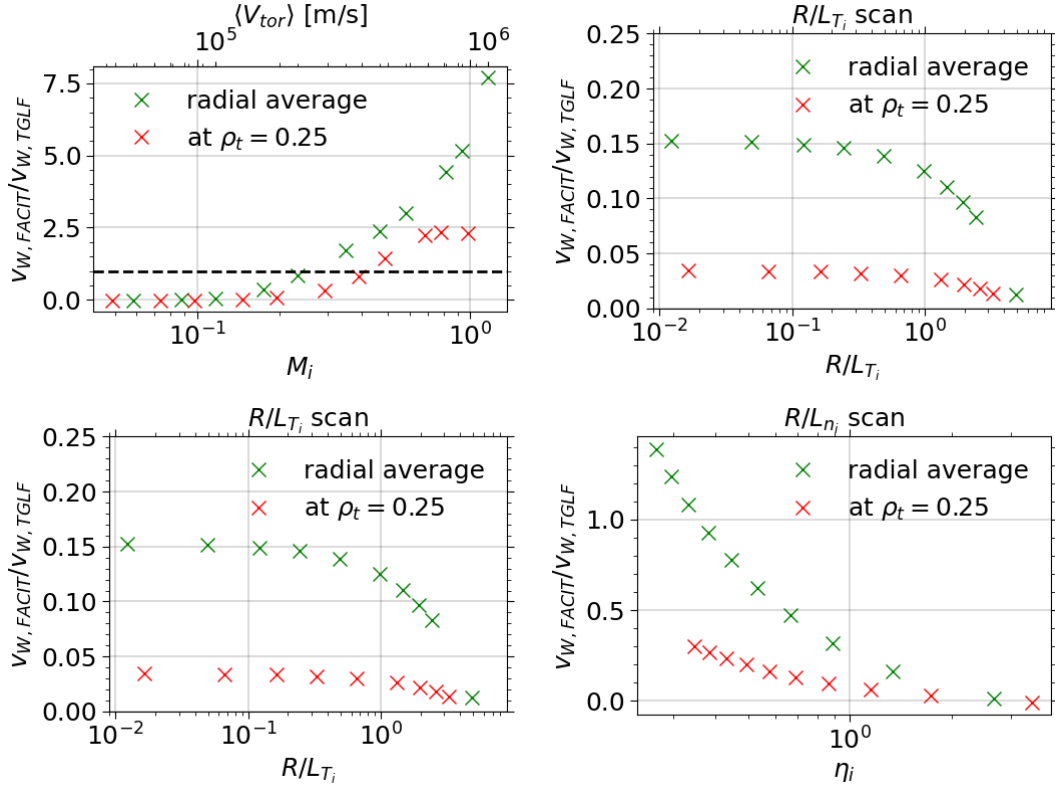


Figure 19: Ratios between W neoclassical and turbulent convection for different FACIT standalone scans. Top left: rotation (and Mach number) scan; top right: R/L_{T_i} scan; bottom: R/L_{n_i} scan. The bottom left (right) plot shows the convection ratio vs R/L_{n_i} (η_i). Red indicates the value at $\rho_t = 0.25$ and green shows the radial average up to the pedestal top.

interesting trends which deserve further explanation. The toroidal velocity scan shows that the neoclassical transport becomes comparable to the turbulent one for Mach ion numbers above 0.25. Although such numbers can be reached in tokamak plasmas, the

figure shows that for this SPARC scenario this would correspond to toroidal velocities bigger than 300 km/s , which is an order of magnitude higher than the maximum values found in the momentum transport simulations shown earlier in this section. The normalized ion temperature gradient scan shows that even approaching near-null values of R/L_{T_i} the ratio between neoclassical and anomalous pinch asymptotically tends to a maximum value of 0.15. Finally, the density gradient scan, shown at the bottom left of the figure, illustrates that the average $v_{W,NC}/v_{W,turb}$ reaches ~ 1 only for unrealistic values of R/L_{n_i} which are an order of magnitude higher than those found in nominal ASTRA flux-matched simulations. For comparison, also $\eta_i = L_{n_i}/L_{T_i}$ is plotted at the bottom right of the figure. The scan highlights how $\eta_i < 0.35$ would be needed to obtain $v_{W,NC} \sim v_{W,turb}$. The results presented in this section demonstrate the robust predominance of anomalous impurity transport, indicating that only unrealistically high toroidal rotation or normalized density gradient values—unlikely to be achieved in reactor-relevant devices—would make neoclassical transport comparable in magnitude.

6. Sensitivity of fusion and impurity peaking to DT fuel mix composition

In the previous simulations, the main ion species has been assumed with a 50-50% DT fuel composition, lumping the D and T masses into a unique species with mass 2.5. However, a different fuel mixture leads to different fusion power, which in turn affects the kinetic profiles. This could indirectly impact the impurity transport, which may provide a different peaking level via diverse turbulent / neoclassical contributions. This argument has motivated additional simulations, performed scanning the D concentration at the top of pedestal and evolving it separately from T as an additional species in ASTRA. Therefore, in the new simulations, electrons, T, He3 and Ar are simulated, D is imposed by quasi-neutrality, and W is not included, due to the limits of 5 species imposed by the present implementation of TGLF in ASTRA. W has been excluded from the simulations because it is the most diluted species in the plasma and Ar is needed to maintain the target Z_{eff} value. The D pedestal concentration (i.e. f_D , with respect to the total D+T density) has been scanned from 0.22 to 0.88. The results are shown in figure 20, while figure 21 shows the D and T densities, together with the kinetic profiles. Figure 20 indicates that the maximum fusion power is around 55-45% DT fuel mix. This result is unexpected and requires further investigation. Interestingly, the dependence of fusion power on f_D is not symmetric with respect to the 50-50% composition. In particular, higher D concentrations give higher fusion power at similar $n_D n_T$ values. Since P_{fus} scales as $n_D n_T T_i^C$, where $C > 0$, this indicates that the DT fuel composition affects the average ion temperature profile, predicting higher values at higher f_D . In order to verify this, the average T_i and its peaking are shown in the right plot of figure 20. The higher ion temperature at higher D concentrations explains why the maximum fusion power is found at 55-45% DT fuel composition. The variation of the T_i profile can be seen in the right plot of figure 21. Figure 22 shows that the Ar density in the inner core increases with f_D , leading to higher Z_{eff} , which in turn affect

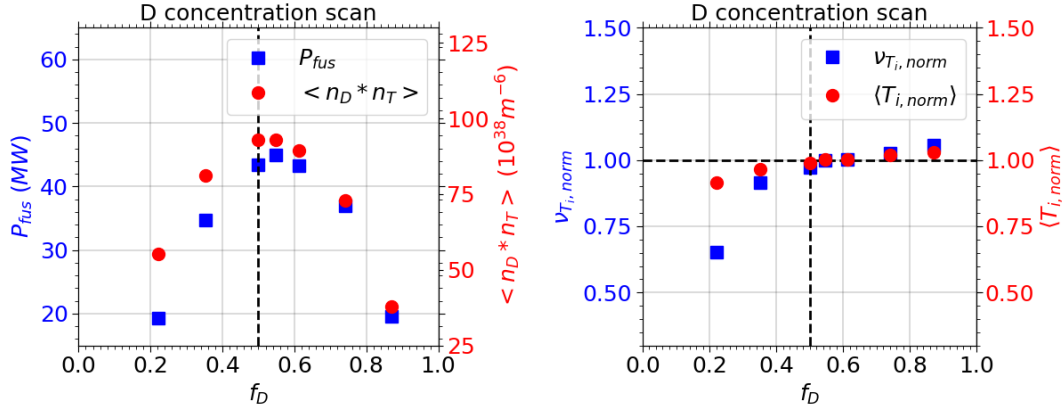


Figure 20: Left: fusion power (blue) and $n_D n_T$ (red) for an H12 scan of D pedestal concentration. Right: average ion temperature (red) and T_i peaking (blue), normalized to the nominal ASTRA case (i.e. 50-50% DT)). For both plots, the X-axis indicates the D concentration at top of pedestal with respect to the total D+T density.

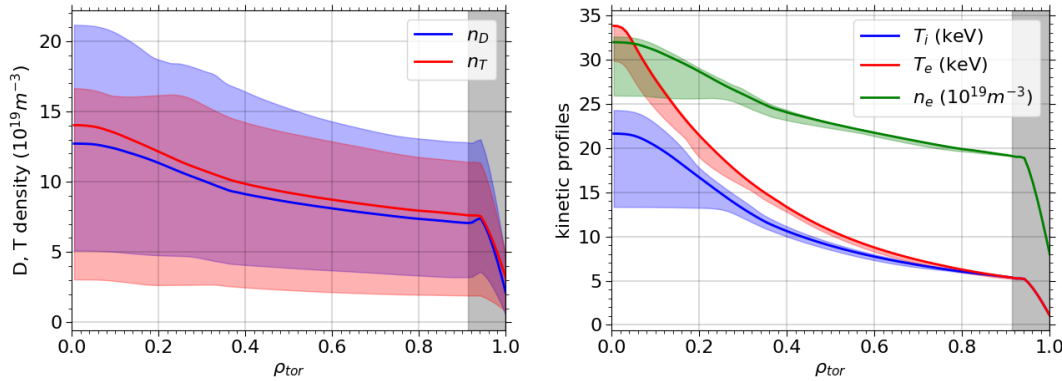


Figure 21: On the left the D (blue) and T (red) density profiles are shown, while on the right the kinetic profiles are pictured. The colored shades indicate the maximum and minimum values computed for the profiles. The gray area is from top of pedestal to the separatrix.

the ITG stability, setting different T_i/T_e values. The effect of increased radiation at higher Ar densities on the electron temperature is negligible, due to its small relative variation and the stiffness of the T_e profile. The difference in the Ar peaking is related to the effect that the main ion mass has on the background turbulence (i.e. isotope effect). In fact, it has been observed that D has a higher turbulent growth rate compared to T, with fixed other conditions [8, 76]. This typically implies a higher heat flux, while its effect on particle fluxes is non-trivial and it depends on the turbulent regime [3, 2, 21]. The bottom right plot of figure 22 shows higher impurity inward convection at higher f_D . A higher D concentration in the fuel mix can be considered similar to a DT lumped species with lower mass. The observed isotope effect on particle transport has been confirmed by standalone TGLF simulations, performed scanning the D concentration

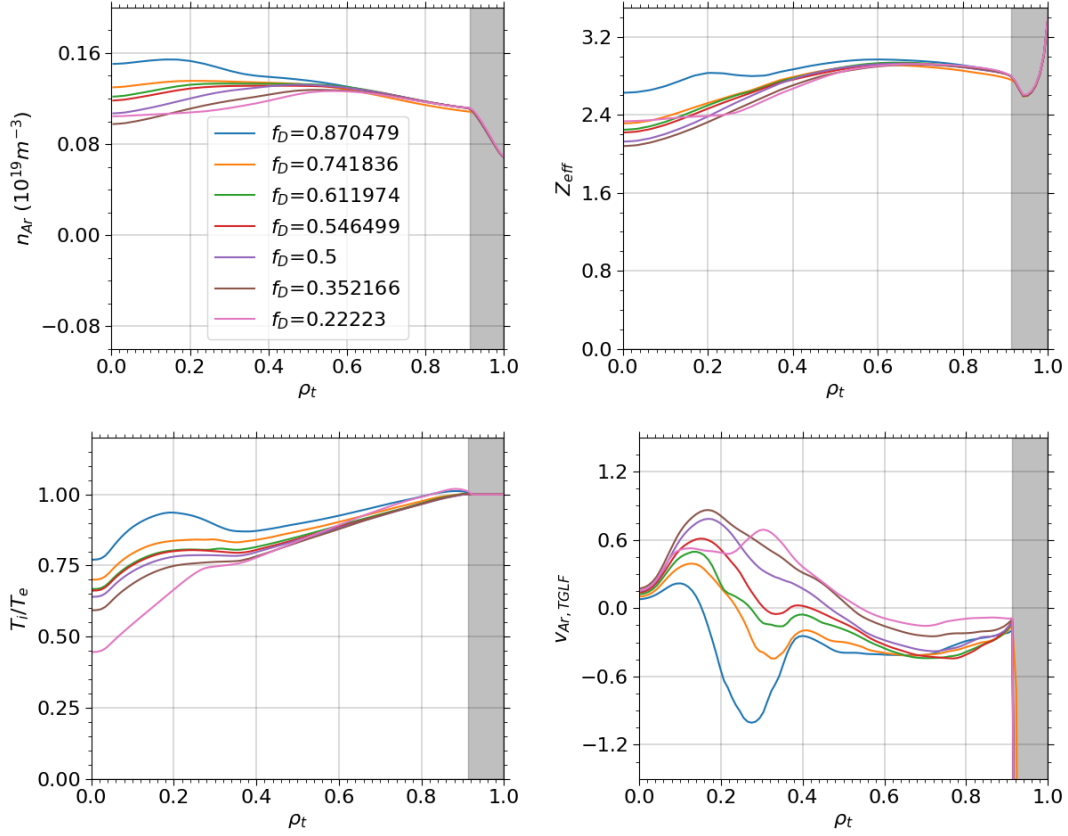


Figure 22: Profiles for a scan in D concentration of the H12 scenario. Top left: Ar density; top right: effective charge; bottom left: ion to electron temperature ratio; bottom right: anomalous Ar convection. The gray area is from top of pedestal to the separatrix.

and enforcing the T density with quasi-neutrality. The results, shown in figure 23, show an ITG-dominated regime, where the Ar outward flux decreases with f_D . The same trend has been observed for the electron particle flux. An additional sensitivity study, varying the Ar density gradient by $\pm 50\%$ has shown an Ar flux variation $< 10\%$, proving the robustness of the results. Since the regime is ITG dominated and the impurity flux decreases at higher linear growth rates, the pure pinch should prevail on thermo-diffusion [3]. These results suggest that if a 55-45% DT fuel mix is not available, higher D concentrations are preferable and can still provide reasonable fusion power. For example a 75-25% DT mix shows 20% higher fusion power compared to 25-75% composition. However, this study does not aim at describing the physics of isotope effect in detail, therefore a more rigorous analysis, e.g. comparing with non linear gyrokinetics and separating the convection in pure pinch, thermo- and roto-diffusion, is beyond the scope of the paper.

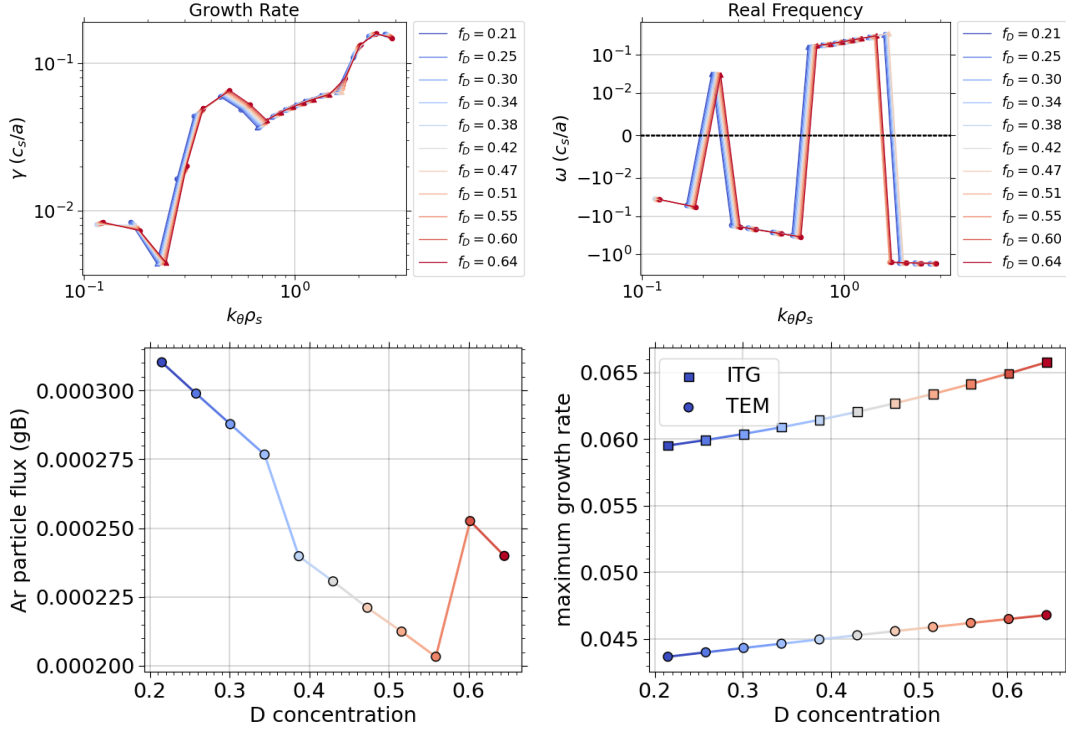


Figure 23: Turbulent spectra and global quantities of TGLF standalone simulations scanning the D concentration (f_D) and modifying the T density to enforce quasi-neutrality. Top left: growth rates; top right: mode frequencies; bottom left: Ar particle flux; bottom right: most unstable ITG and TEM growth rates. Different colors are for different f_D values.

7. Conclusions

In this paper, the impurity transport for three SPARC H-modes has been investigated. The results have shown that the turbulence dominates over the neoclassical contribution for Ar and W impurities. A successful benchmark with previously published simulations has been provided, highlighting that the assumption of flat impurity concentrations is a reasonable approach to quantify fusion performance variations in extensive databases. Such evidence has been shown at different values of ICRH input power and top of pedestal densities. The modeling used in this paper assumed an ad-hoc edge transport to set impurity concentrations as boundary conditions at the top of pedestal. This choice is imposed by the lack of accurate turbulent model in stiff H-mode pedestals, but the precise value of pedestal concentrations is uncertain. Therefore, the low current H-mode scenario has been selected to perform scans of Ar and W source, which determined different boundary conditions at pedestal, covering a wide and conservative range. The results showed a minimal impact of W concentration variations on the impurity profiles. On the other hand, the Ar source scan has shown an interesting non-trivial interplay between different effects, including pedestal pressure, density peaking and DT dilution,

which counterbalanced each other resulting in the plasma performance being insensitive to the Ar concentration and the associated Z_{eff} . Most of the performed simulations assumed null rotation. Without external torque sources, this is a reasonable assumption for SPARC, which will operate without Neutral Beam Injection. However, rotation has been observed to have an impact on both turbulent and neoclassical transport. Therefore, a set of ASTRA simulations including a reduced model for core rotation has been used, varying a constant edge toroidal velocity in a wide range as boundary condition for core calculations. The results have shown minimal impact on the electron, main ion and impurities profiles. In order to assess the robustness of these predictions, additional scans of FACIT standalone have been performed, to determine variables ranges in which the neoclassical impurity transport becomes competitive with the turbulent one. The variation of normalized T_i gradient has shown that even assuming flat profile will give a maximum contribution of neoclassical transport of about 15%. However, high fusion conditions should lead to significant power flow and relatively peaked temperature profiles. The scan in normalized n_i gradient has shown that the neoclassical transport becomes comparable with the turbulent one only at $R/L_{ne} > 12$, which is unrealistic. The scan in toroidal velocity revealed that the transport coefficients calculated by FACIT reach TGLF values only above 200km/s (i.e. Mach number 0.2), which is one order of magnitude higher than the maximum value found in ASTRA. Such a high rotation seems unrealistic for the analyzed scenario. All the simulations performed in the paper, including the latest sensitivity scans, showed that the turbulent W transport is robustly higher than the neoclassical component, across multiple variations of uncertain parameters. These findings align with ITER predictions from existing literature [24]. Finally, an additional study has been performed to study the effect of assuming different DT fuel mix compositions on the impurity transport and plasma performance. Surprisingly, the maximum fusion power has been found at 55-45% DT fuel mix composition, with high D concentrations preferable with respect to symmetrically high T concentrations. This unexpected result comes from the isotope effect on impurity transport. In particular, higher D concentrations showed higher linear growth rates, which in the ITG dominated regime studied here increased the Ar pinch, leading to higher Z_{eff} and ion temperature peaking.

Acknowledgments

The authors thank the MIT PSFC for its constructive feedback, in particular the MFE Integrated Modeling group, John Wright for technical support about computational resources and Conor Perks for interesting discussions about impurity transport. The authors thank Teobaldo Luda, Michael Bergmann and Emiliano Fable for sharing their experiences with the ASTRA code. The authors acknowledge the use of ChatGPT during the article editing phase. This research used resources of the National Energy Research Scientific Computing Center, a DOE Office of Science User Facility using NERSC award FES-ERCAP0032161, for the EPED simulations used to train the neural network model. The ASTRA simulations (ASTRA from main branch with hash a00f496a5489e12bbdbdc02dc38482057dd43b0b) presented in this paper were performed on the MIT-PSFC partition of the Engaging cluster at the MGHPC facility (www.mghpcc.org) which was funded by DoE grant number DE-FG02-91-ER54109.

This work was supported by CFS under RPP020 fundings.

References

- [1] C Angioni and P Helander. “Neoclassical transport of heavy impurities with poloidally asymmetric density distribution in tokamaks”. In: *Plasma Physics and Controlled Fusion* 56.12 (Dec. 2014), p. 124001. ISSN: 0741-3335, 1361-6587. DOI: 10.1088/0741-3335/56/12/124001. URL: <https://iopscience.iop.org/article/10.1088/0741-3335/56/12/124001> (visited on 10/24/2025).
- [2] C Angioni et al. “Particle transport in tokamak plasmas, theory and experiment”. In: *Plasma Physics and Controlled Fusion* 51.12 (Dec. 2009), p. 124017. ISSN: 0741-3335, 1361-6587. DOI: 10.1088/0741-3335/51/12/124017. URL: <https://iopscience.iop.org/article/10.1088/0741-3335/51/12/124017> (visited on 10/28/2025).
- [3] C. Angioni and A. G. Peeters. “Direction of Impurity Pinch and Auxiliary Heating in Tokamak Plasmas”. en. In: *Physical Review Letters* 96.9 (Mar. 2006), p. 095003. ISSN: 0031-9007, 1079-7114. DOI: 10.1103/PhysRevLett.96.095003. URL: <https://link.aps.org/doi/10.1103/PhysRevLett.96.095003> (visited on 10/28/2025).
- [4] C. Angioni et al. “Confinement properties of L-mode plasmas in ASDEX Upgrade and full-radius predictions of the TGLF transport model”. In: *Nuclear Fusion* 62.6 (June 2022), p. 066015. ISSN: 0029-5515, 1741-4326. DOI: 10.1088/1741-4326/ac592b. URL: <https://iopscience.iop.org/article/10.1088/1741-4326/ac592b> (visited on 12/02/2024).

- [5] B Baiocchi et al. “Turbulent transport analysis of JET H-mode and hybrid plasmas using QuaLiKiz and Trapped Gyro Landau Fluid”. In: *Plasma Physics and Controlled Fusion* 57.3 (Mar. 2015), p. 035003. ISSN: 0741-3335, 1361-6587. DOI: 10.1088/0741-3335/57/3/035003. URL: <https://iopscience.iop.org/article/10.1088/0741-3335/57/3/035003> (visited on 12/02/2024).
- [6] M. Barnes et al. “Turbulent Transport in Tokamak Plasmas with Rotational Shear”. en. In: *Physical Review Letters* 106.17 (Apr. 2011), p. 175004. ISSN: 0031-9007, 1079-7114. DOI: 10.1103/PhysRevLett.106.175004. URL: <https://link.aps.org/doi/10.1103/PhysRevLett.106.175004> (visited on 10/28/2025).
- [7] C. F. Barnett and M. F. A. Harrison. *Plasmas: Applied Atomic Collision Physics, Vol. 2*. eng. Burlington: Elsevier Science, 2013. ISBN: 9780124788022.
- [8] E. A. Belli and J. Candy. “Asymmetry between deuterium and tritium turbulent particle flows”. en. In: *Physics of Plasmas* 28.6 (June 2021), p. 062301. ISSN: 1070-664X, 1089-7674. DOI: 10.1063/5.0048620. URL: <https://pubs.aip.org/pop/article/28/6/062301/973253/Asymmetry-between-deuterium-and-tritium-turbulent> (visited on 10/28/2025).
- [9] C. Bourdelle et al. “A new gyrokinetic quasilinear transport model applied to particle transport in tokamak plasmas”. en. In: *Physics of Plasmas* 14.11 (Nov. 2007), p. 112501. ISSN: 1070-664X, 1089-7674. DOI: 10.1063/1.2800869. URL: <https://pubs.aip.org/pop/article/14/11/112501/936423/A-new-gyrokinetic-quasilinear-transport-model> (visited on 10/24/2025).
- [10] M Brambilla. “Numerical simulation of ion cyclotron waves in tokamak plasmas”. In: *Plasma Physics and Controlled Fusion* 41.1 (Jan. 1999), pp. 1–34. ISSN: 0741-3335, 1361-6587. DOI: 10.1088/0741-3335/41/1/002. URL: <https://iopscience.iop.org/article/10.1088/0741-3335/41/1/002> (visited on 11/19/2024).
- [11] Y. Camenen et al. “Impact of the background toroidal rotation on particle and heat turbulent transport in tokamak plasmas”. en. In: *Physics of Plasmas* 16.1 (Jan. 2009), p. 012503. ISSN: 1070-664X, 1089-7674. DOI: 10.1063/1.3057356. URL: <https://pubs.aip.org/pop/article/16/1/012503/261676/Impact-of-the-background-toroidal-rotation-on> (visited on 10/28/2025).
- [12] J. Candy and R.E. Waltz. “An Eulerian gyrokinetic-Maxwell solver”. en. In: *Journal of Computational Physics* 186.2 (Apr. 2003), pp. 545–581. ISSN: 00219991. DOI: 10.1016/S0021-9991(03)00079-2. URL: <https://linkinghub.elsevier.com/retrieve/pii/S0021999103000792> (visited on 12/06/2024).
- [13] F J Casson et al. “Theoretical description of heavy impurity transport and its application to the modelling of tungsten in JET and ASDEX upgrade”. In: *Plasma Physics and Controlled Fusion* 57.1 (Jan. 2015), p. 014031. ISSN: 0741-3335, 1361-6587. DOI: 10.1088/0741-3335/57/1/014031. URL: <https://iopscience.iop.org/article/10.1088/0741-3335/57/1/014031> (visited on 10/24/2025).

- [14] M.D. Clement, N.C. Logan, and M.D. Boyer. “Neoclassical toroidal viscosity torque prediction via deep learning”. In: *Nuclear Fusion* 62.2 (Feb. 2022), p. 026022. ISSN: 0029-5515, 1741-4326. DOI: 10.1088/1741-4326/ac3e83. URL: <https://iopscience.iop.org/article/10.1088/1741-4326/ac3e83> (visited on 11/04/2025).
- [15] A. J. Creely et al. “Overview of the SPARC tokamak”. en. In: *Journal of Plasma Physics* 86.5 (Oct. 2020), p. 865860502. ISSN: 0022-3778, 1469-7807. DOI: 10.1017/S0022377820001257. URL: https://www.cambridge.org/core/product/identifier/S0022377820001257/type/journal%5C_article (visited on 11/19/2024).
- [16] A. J. Creely et al. “Validation of nonlinear gyrokinetic simulations of L- and I-mode plasmas on Alcator C-Mod”. en. In: *Physics of Plasmas* 24.5 (May 2017), p. 056104. ISSN: 1070-664X, 1089-7674. DOI: 10.1063/1.4977466. URL: <https://pubs.aip.org/pop/article/24/5/056104/991885/Validation-of-nonlinear-gyrokinetic-simulations-of> (visited on 05/12/2025).
- [17] A. Di Siena et al. “Global gyrokinetic simulations of ASDEX Upgrade up to the transport timescale with GENE–Tango”. In: *Nuclear Fusion* 62.10 (Oct. 2022), p. 106025. ISSN: 0029-5515, 1741-4326. DOI: 10.1088/1741-4326/ac8941. URL: <https://iopscience.iop.org/article/10.1088/1741-4326/ac8941> (visited on 10/24/2025).
- [18] A. M. Dimits et al. “Comparisons and physics basis of tokamak transport models and turbulence simulations”. en. In: *Physics of Plasmas* 7.3 (Mar. 2000), pp. 969–983. ISSN: 1070-664X, 1089-7674. DOI: 10.1063/1.873896. URL: <https://pubs.aip.org/pop/article/7/3/969/1029781/Comparisons-and-physics-basis-of-tokamak-transport> (visited on 12/06/2024).
- [19] Ralph Dux. *STRAHL User Manual*. Tech. rep. 10/30. IPP–10/30. Germany, 2006.
- [20] P. Ennever et al. “The effects of dilution on turbulence and transport in C-Mod ohmic plasmas and comparisons with gyrokinetic simulations”. en. In: *Physics of Plasmas* 22.7 (July 2015), p. 072507. ISSN: 1070-664X, 1089-7674. DOI: 10.1063/1.4926518. URL: <https://pubs.aip.org/pop/article/22/7/072507/264325/The-effects-of-dilution-on-turbulence-and> (visited on 11/19/2024).
- [21] E Fable, C Angioni, and O Sauter. “The role of ion and electron electrostatic turbulence in characterizing stationary particle transport in the core of tokamak plasmas”. In: *Plasma Physics and Controlled Fusion* 52.1 (Jan. 2010), p. 015007. ISSN: 0741-3335, 1361-6587. DOI: 10.1088/0741-3335/52/1/015007. URL: <https://iopscience.iop.org/article/10.1088/0741-3335/52/1/015007> (visited on 10/28/2025).
- [22] D Fajardo et al. “Analytical model for collisional impurity transport in tokamaks at arbitrary collisionality”. In: *Plasma Physics and Controlled Fusion* 64.5 (May 2022), p. 055017. ISSN: 0741-3335, 1361-6587. DOI: 10.1088/1361-6587/ac5b4d.

- URL: <https://iopscience.iop.org/article/10.1088/1361-6587/ac5b4d> (visited on 10/24/2025).
- [23] D Fajardo et al. “Analytical model for the combined effects of rotation and collisionality on neoclassical impurity transport”. In: *Plasma Physics and Controlled Fusion* 65.3 (Mar. 2023), p. 035021. ISSN: 0741-3335, 1361-6587. DOI: 10.1088/1361-6587/acb0fc. URL: <https://iopscience.iop.org/article/10.1088/1361-6587/acb0fc> (visited on 10/24/2025).
- [24] D Fajardo et al. “Theory-based integrated modelling of tungsten transport in ITER plasmas”. In: *Plasma Physics and Controlled Fusion* 67.1 (Jan. 2025), p. 015020. ISSN: 0741-3335, 1361-6587. DOI: 10.1088/1361-6587/ad9aca. URL: <https://iopscience.iop.org/article/10.1088/1361-6587/ad9aca> (visited on 10/24/2025).
- [25] D. Fajardo et al. “Full-radius integrated modelling of ASDEX Upgrade L-modes including impurity transport and radiation”. In: *Nuclear Fusion* 64.4 (Apr. 2024), p. 046021. ISSN: 0029-5515, 1741-4326. DOI: 10.1088/1741-4326/ad29bd. URL: <https://iopscience.iop.org/article/10.1088/1741-4326/ad29bd> (visited on 10/24/2025).
- [26] D. Fajardo et al. “Integrated modelling of tungsten accumulation control with wave heating: validation in ASDEX Upgrade and predictions for ITER”. In: *Nuclear Fusion* 64.10 (Oct. 2024), p. 104001. ISSN: 0029-5515, 1741-4326. DOI: 10.1088/1741-4326/ad6f26. URL: <https://iopscience.iop.org/article/10.1088/1741-4326/ad6f26> (visited on 12/06/2024).
- [27] C. Fenzi et al. “On plasma rotation with toroidal magnetic field ripple and no external momentum input”. In: *Nuclear Fusion* 51.10 (Oct. 2011), p. 103038. ISSN: 0029-5515, 1741-4326. DOI: 10.1088/0029-5515/51/10/103038. URL: <https://iopscience.iop.org/article/10.1088/0029-5515/51/10/103038> (visited on 11/04/2025).
- [28] *freegs-plasma/freegs*. original-date: 2016-11-15T11:28:29Z. Nov. 2024. URL: <https://github.com/freegs-plasma/freegs> (visited on 12/06/2024).
- [29] Xavier Garbet. “Introduction to turbulent transport in fusion plasmas”. en. In: *Comptes Rendus. Physique* 7.6 (July 2006), pp. 573–583. ISSN: 1878-1535. DOI: 10.1016/j.crhy.2006.06.002. URL: <https://comptes-rendus.academie-sciences.fr/physique/articles/10.1016/j.crhy.2006.06.002/> (visited on 12/06/2024).
- [30] Harold Grad and Hanan Rubin. “HYDROMAGNETIC EQUILIBRIA AND FORCE-FREE FIELDS”. In: *Journal of Nuclear Energy* 7 (1958), pp. 284–285. URL: <https://api.semanticscholar.org/CorpusID:121009637>.
- [31] V. Grandgirard et al. “A drift-kinetic Semi-Lagrangian 4D code for ion turbulence simulation”. en. In: *Journal of Computational Physics* 217.2 (Sept. 2006), pp. 395–423. ISSN: 00219991. DOI: 10.1016/j.jcp.2006.01.023. URL: <https://>

- linkinghub.elsevier.com/retrieve/pii/S0021999106000155 (visited on 12/06/2024).
- [32] W. Guttenfelder et al. “Predictions of core plasma performance for the Infinity Two fusion pilot plant”. en. In: *Journal of Plasma Physics* 91.3 (June 2025), E83. ISSN: 0022-3778, 1469-7807. DOI: 10.1017/S0022377825000339. URL: <https://www.cambridge.org/core/journals/journal-of-plasma-physics/article/predictions-of-core-plasma-performance-for-the-infinity-two-fusion-pilot-plant/707D1908C7D42B614D5561987EA7E16D> (visited on 10/24/2025).
- [33] G W Hammett. “Fast ion studies of ion cyclotron heating in the PLT tokamak”. English. PhD thesis. United States: Princeton Univ., Princeton, NJ, Jan. 1986. URL: <https://www.osti.gov/biblio/5079411>.
- [34] A. Ho et al. “Neural network surrogate of QuaLiKiz using JET experimental data to populate training space”. In: *Physics of Plasmas* 28.3 (2021), p. 032305. DOI: 10.1063/5.0038290.
- [35] Suk-Ho Hong. “A review of DEMO reactor concepts: open questions and issues”. en. In: *AAPPS Bulletin* 32.1 (Dec. 2022), p. 10. ISSN: 2309-4710. DOI: 10.1007/s43673-022-00040-9. URL: <https://link.springer.com/10.1007/s43673-022-00040-9> (visited on 12/02/2025).
- [36] W.A. Houlberg, S.E. Attenberger, and L.M. Hively. “Contour analysis of fusion reactor plasma performance”. In: *Nuclear Fusion* 22.7 (July 1982), pp. 935–945. ISSN: 0029-5515, 1741-4326. DOI: 10.1088/0029-5515/22/7/006. URL: <https://iopscience.iop.org/article/10.1088/0029-5515/22/7/006> (visited on 12/06/2024).
- [37] N. T. Howard et al. “Gyrokinetic simulation of turbulence and transport in the SPARC tokamak”. en. In: *Physics of Plasmas* 28.7 (July 2021), p. 072502. ISSN: 1070-664X, 1089-7674. DOI: 10.1063/5.0047789. URL: <https://pubs.aip.org/pop/article/28/7/072502/594534/Gyrokinetic-simulation-of-turbulence-and-transport> (visited on 12/03/2025).
- [38] F Imbeaux, F Ryter, and X Garbet. “Modelling of ECH modulation experiments in ASDEX Upgrade with an empirical critical temperature gradient length transport model”. In: *Plasma Physics and Controlled Fusion* 43.11 (Nov. 2001), pp. 1503–1524. ISSN: 0741-3335, 1361-6587. DOI: 10.1088/0741-3335/43/11/306. URL: <https://iopscience.iop.org/article/10.1088/0741-3335/43/11/306> (visited on 12/09/2024).
- [39] AA Ivanov. *New adaptive grid plasma evolution code SPIDER*. In Europhysics Conference Abstracts Vol. 29C, ISBN 2-914771-24-X. Tarragona, 2005.
- [40] F. Jenko, W. Dorland, and G. W. Hammett. “Critical gradient formula for toroidal electron temperature gradient modes”. en. In: *Physics of Plasmas* 8.9 (Sept. 2001), pp. 4096–4104. ISSN: 1070-664X, 1089-7674. DOI: 10.1063/1.1391261. URL:

- <https://pubs.aip.org/pop/article/8/9/4096/265245/Critical-gradient-formula-for-toroidal-electron> (visited on 11/19/2024).
- [41] Frank Jenko. “Massively parallel Vlasov simulation of electromagnetic drift-wave turbulence”. en. In: *Computer Physics Communications* 125.1-3 (Mar. 2000), pp. 196–209. ISSN: 00104655. DOI: 10.1016/S0010-4655(99)00489-0. URL: <https://linkinghub.elsevier.com/retrieve/pii/S0010465599004890> (visited on 12/06/2024).
- [42] B. B. Kadomtsev. “Disruptive instability in Tokamaks”. In: *Fizika Plazmy* 1 (Sept. 1975). ADS Bibcode: 1975FizPl...1..710K, pp. 710–715. URL: <https://ui.adsabs.harvard.edu/abs/1975FizPl...1..710K> (visited on 11/19/2024).
- [43] A Kallenbach et al. “Impurity seeding for tokamak power exhaust: from present devices via ITER to DEMO”. In: *Plasma Physics and Controlled Fusion* 55.12 (Dec. 2013), p. 124041. ISSN: 0741-3335, 1361-6587. DOI: 10.1088/0741-3335/55/12/124041. URL: <https://iopscience.iop.org/article/10.1088/0741-3335/55/12/124041> (visited on 10/24/2025).
- [44] Kyuho Kim et al. “Full-f XGC1 gyrokinetic study of improved ion energy confinement from impurity stabilization of ITG turbulence”. en. In: *Physics of Plasmas* 24.6 (June 2017), p. 062302. ISSN: 1070-664X, 1089-7674. DOI: 10.1063/1.4984991. URL: <https://pubs.aip.org/pop/article/24/6/062302/108560/Full-f-XGC1-gyrokinetic-study-of-improved-ion> (visited on 12/06/2024).
- [45] J. E. Kinsey, R. E. Waltz, and J. Candy. “Nonlinear gyrokinetic turbulence simulations of $E \times B$ shear quenching of transport”. en. In: *Physics of Plasmas* 12.6 (June 2005), p. 062302. ISSN: 1070-664X, 1089-7674. DOI: 10.1063/1.1920327. URL: <https://pubs.aip.org/pop/article/12/6/062302/762149/Nonlinear-gyrokinetic-turbulence-simulations-of-E> (visited on 10/28/2025).
- [46] M. Kotschenreuther et al. “Gyrokinetic analysis and simulation of pedestals to identify the culprits for energy losses using ‘fingerprints’”. In: *Nuclear Fusion* 59.9 (Sept. 2019), p. 096001. ISSN: 0029-5515, 1741-4326. DOI: 10.1088/1741-4326/ab1fa2. URL: <https://iopscience.iop.org/article/10.1088/1741-4326/ab1fa2> (visited on 12/04/2025).
- [47] Mike Kotschenreuther, G. Rewoldt, and W.M. Tang. “Comparison of initial value and eigenvalue codes for kinetic toroidal plasma instabilities”. en. In: *Computer Physics Communications* 88.2-3 (Aug. 1995), pp. 128–140. ISSN: 00104655. DOI: 10.1016/0010-4655(95)00035-E. URL: <https://linkinghub.elsevier.com/retrieve/pii/001046559500035E> (visited on 12/06/2024).
- [48] S. I. Krasheninnikov and A. S. Kukushkin. “Physics of ultimate detachment of a tokamak divertor plasma”. en. In: *Journal of Plasma Physics* 83.5 (Oct. 2017), p. 155830501. ISSN: 0022-3778, 1469-7807. DOI: 10.1017/S0022377817000654. URL: https://www.cambridge.org/core/product/identifier/S0022377817000654/type/journal_article (visited on 10/24/2025).

- [49] A.Q. Kuang et al. “Conceptual design study for heat exhaust management in the ARC fusion pilot plant”. en. In: *Fusion Engineering and Design* 137 (Dec. 2018), pp. 221–242. ISSN: 09203796. DOI: 10.1016/j.fusengdes.2018.09.007. URL: <https://linkinghub.elsevier.com/retrieve/pii/S0920379618306185> (visited on 12/02/2025).
- [50] Y. Lin, J. C. Wright, and S. J. Wukitch. “Physics basis for the ICRF system of the SPARC tokamak”. en. In: *Journal of Plasma Physics* 86.5 (Oct. 2020), p. 865860506. ISSN: 0022-3778, 1469-7807. DOI: 10.1017/S0022377820001269. URL: https://www.cambridge.org/core/product/identifier/S0022377820001269/type/journal%5C_article (visited on 12/06/2024).
- [51] A Loarte et al. “The new ITER baseline, research plan and open R&D issues”. In: *Plasma Physics and Controlled Fusion* 67.6 (June 2025), p. 065023. ISSN: 0741-3335, 1361-6587. DOI: 10.1088/1361-6587/add9c9. URL: <https://iopscience.iop.org/article/10.1088/1361-6587/add9c9> (visited on 12/02/2025).
- [52] Y R Martin, T Takizuka, and the ITPA CDBM H-mode Threshold Data Group. “Power requirement for accessing the H-mode in ITER”. In: *Journal of Physics: Conference Series* 123 (July 2008), p. 012033. ISSN: 1742-6596. DOI: 10.1088/1742-6596/123/1/012033. URL: <https://iopscience.iop.org/article/10.1088/1742-6596/123/1/012033> (visited on 08/13/2020).
- [53] R. M. McDermott. “Edge radial electric field studies via charge exchange recombination spectroscopy on the Alcator C-Mod Tokamak”. eng. Thesis. Massachusetts Institute of Technology, 2009. URL: <https://dspace.mit.edu/handle/1721.1/54462> (visited on 11/04/2025).
- [54] O. Meneghini et al. “Neural-network accelerated coupled core-pedestal simulations with self-consistent transport of impurities and compatible with ITER IMAS”. In: *Nuclear Fusion* 61.2 (Dec. 2020). Publisher: IOP Publishing, p. 026006. DOI: 10.1088/1741-4326/abb918.
- [55] O. Meneghini et al. “Self-consistent core-pedestal transport simulations with neural network accelerated models”. In: *Nuclear Fusion* 57.8 (July 2017). Publisher: IOP Publishing, p. 086034. DOI: 10.1088/1741-4326/aa7776.
- [56] M. Muraca et al. “Integrated modeling of SPARC H-mode scenarios: exploration of the impact of modeling assumptions on predicted performance”. In: *Nuclear Fusion* 65.9 (Sept. 2025), p. 096010. ISSN: 0029-5515, 1741-4326. DOI: 10.1088/1741-4326/adf656. URL: <https://iopscience.iop.org/article/10.1088/1741-4326/adf656> (visited on 12/02/2025).
- [57] A. Y Pankin et al. *TRANSP integrated modeling code for interpretive and predictive analysis of tokamak plasmas*. 2024. DOI: 10.48550/ARXIV.2406.07781. URL: <https://arxiv.org/abs/2406.07781> (visited on 11/19/2024).

- [58] A. Y. Pankin et al. “TRANSP integrated modeling code for interpretive and predictive analysis of tokamak plasmas”. In: *Computer Physics Communications* 312 (July 2025), p. 109611. ISSN: 0010-4655. DOI: 10.1016/j.cpc.2025.109611. URL: <https://www.sciencedirect.com/science/article/pii/S0010465525001134> (visited on 07/09/2025).
- [59] Jong-Kyu Park and Nikolas C. Logan. “Self-consistent perturbed equilibrium with neoclassical toroidal torque in tokamaks”. en. In: *Physics of Plasmas* 24.3 (Mar. 2017), p. 032505. ISSN: 1070-664X, 1089-7674. DOI: 10.1063/1.4977898. URL: <https://pubs.aip.org/pop/article/24/3/032505/319136/Self-consistent-perturbed-equilibrium-with> (visited on 11/04/2025).
- [60] A. G. Peeters and D. Strintzi. “The effect of a uniform radial electric field on the toroidal ion temperature gradient mode”. en. In: *Physics of Plasmas* 11.8 (Aug. 2004), pp. 3748–3751. ISSN: 1070-664X, 1089-7674. DOI: 10.1063/1.1762876. URL: <https://pubs.aip.org/pop/article/11/8/3748/261917/The-effect-of-a-uniform-radial-electric-field-on> (visited on 12/06/2024).
- [61] G.V. Pereverzev et al. *ASTRA - an automatic system for transport analysis in a tokamak*. Tech. rep. IPP-5/42 INIS Reference Number: 23024293. Germany, 1991, p. 64.
- [62] Gregorij V Pereverzev and PN Yushmanov. *ASTRA. Automated system for transport analysis in a tokamak*. Tech. rep. 5/98. Max-Planck-Institut für Plasmaphysik, Feb. 2002.
- [63] F. Porcelli, D. Boucher, and M. N. Rosenbluth. “Model for the sawtooth period and amplitude”. en. In: *Plasma Physics and Controlled Fusion* 38.12 (Dec. 1996), p. 2163. ISSN: 0741-3335. DOI: 10.1088/0741-3335/38/12/010. URL: <https://dx.doi.org/10.1088/0741-3335/38/12/010> (visited on 06/27/2023).
- [64] D.E. Post et al. “Steady-state radiative cooling rates for low-density, high-temperature plasmas”. en. In: *Atomic Data and Nuclear Data Tables* 20.5 (Nov. 1977), pp. 397–439. ISSN: 0092640X. DOI: 10.1016/0092-640X(77)90026-2. URL: <https://linkinghub.elsevier.com/retrieve/pii/0092640X77900262> (visited on 10/29/2025).
- [65] T. Pütterich et al. “Calculation and experimental test of the cooling factor of tungsten”. In: *Nuclear Fusion* 50.2 (Feb. 2010), p. 025012. ISSN: 0029-5515, 1741-4326. DOI: 10.1088/0029-5515/50/2/025012. URL: <https://iopscience.iop.org/article/10.1088/0029-5515/50/2/025012> (visited on 10/29/2025).
- [66] P. Rodriguez-Fernandez, N. T. Howard, and J. Candy. “Nonlinear gyrokinetic predictions of SPARC burning plasma profiles enabled by surrogate modeling”. en. In: *Nuclear Fusion* 62.7 (May 2022). Publisher: IOP Publishing, p. 076036. ISSN: 0029-5515. DOI: 10.1088/1741-4326/ac64b2. URL: <https://dx.doi.org/10.1088/1741-4326/ac64b2> (visited on 05/29/2024).

- [67] P. Rodriguez-Fernandez et al. “Core performance predictions in projected SPARC first-campaign plasmas with nonlinear CGYRO”. In: *Physics of Plasmas* 31.6 (June 2024), p. 062501. ISSN: 1070-664X. DOI: 10.1063/5.0209752. URL: <https://doi.org/10.1063/5.0209752> (visited on 06/04/2024).
- [68] P. Rodriguez-Fernandez et al. “Enhancing predictive capabilities in fusion burning plasmas through surrogate-based optimization in core transport solvers”. en. In: *Nuclear Fusion* 64.7 (June 2024). Publisher: IOP Publishing, p. 076034. ISSN: 0029-5515. DOI: 10.1088/1741-4326/ad4b3d. URL: <https://dx.doi.org/10.1088/1741-4326/ad4b3d> (visited on 07/30/2024).
- [69] P. Rodriguez-Fernandez et al. “Perturbative transport modeling of cold-pulse dynamics in Alcator C-Mod Ohmic plasmas”. In: *Nuclear Fusion* 59.6 (June 2019), p. 066017. ISSN: 0029-5515, 1741-4326. DOI: 10.1088/1741-4326/ab1575. URL: <https://iopscience.iop.org/article/10.1088/1741-4326/ab1575> (visited on 12/02/2024).
- [70] P. Rodriguez-Fernandez et al. “Predict-first experiments and modeling of perturbative cold pulses in the DIII-D tokamak”. en. In: *Physics of Plasmas* 26.6 (June 2019), p. 062503. ISSN: 1070-664X, 1089-7674. DOI: 10.1063/1.5096800. URL: <https://pubs.aip.org/pop/article/26/6/062503/1061751/Predict-first-experiments-and-modeling-of> (visited on 12/02/2024).
- [71] P. Rodriguez-Fernandez et al. “Predictions of core plasma performance for the SPARC tokamak”. en. In: *Journal of Plasma Physics* 86.5 (Oct. 2020), p. 865860503. ISSN: 0022-3778, 1469-7807. DOI: 10.1017/S0022377820001075. URL: https://www.cambridge.org/core/product/identifier/S0022377820001075/type/journal%5C_article (visited on 12/06/2024).
- [72] Michele Romanelli et al. “JINTRAC: A System of Codes for Integrated Simulation of Tokamak Scenarios”. en. In: *Plasma and Fusion Research* 9.0 (2014), pp. 3403023–3403023. ISSN: 1880-6821. DOI: 10.1585/pfr.9.3403023. URL: https://www.jstage.jst.go.jp/article/pfr/9/0/9_3403023/_article (visited on 10/24/2025).
- [73] F Ryter et al. “Electron heat transport in ASDEX Upgrade: experiment and modelling”. In: *Nuclear Fusion* 43.11 (Nov. 2003), pp. 1396–1404. ISSN: 0029-5515, 1741-4326. DOI: 10.1088/0029-5515/43/11/011. URL: <https://iopscience.iop.org/article/10.1088/0029-5515/43/11/011> (visited on 12/09/2024).
- [74] M. Schmidtmayr et al. “Investigation of the critical edge ion heat flux for L-H transitions in Alcator C-Mod and its dependence on B_T ”. In: *Nuclear Fusion* 58.5 (May 2018), p. 056003. ISSN: 0029-5515, 1741-4326. DOI: 10.1088/1741-4326/aaaed0. URL: <https://iopscience.iop.org/article/10.1088/1741-4326/aaaed0> (visited on 11/19/2024).
- [75] V. D. Shafranov. “Plasma Equilibrium in a Magnetic Field”. In: *Reviews of Plasma Physics* 2 (Jan. 1966), p. 103.

- [76] G. Snoep et al. *Characterization of reduced-order turbulence models in the L-mode pedestal-forming region in JET*. 2025. DOI: 10.48550/ARXIV.2506.03459. URL: <https://arxiv.org/abs/2506.03459> (visited on 10/28/2025).
- [77] P. B. Snyder et al. “A first-principles predictive model of the pedestal height and width: development, testing and ITER optimization with the EPED model”. en. In: *Nuclear Fusion* 51.10 (Aug. 2011), p. 103016. ISSN: 0029-5515. DOI: 10.1088/0029-5515/51/10/103016. URL: <https://dx.doi.org/10.1088/0029-5515/51/10/103016> (visited on 06/13/2023).
- [78] B.N. Sorbom et al. “ARC: A compact, high-field, fusion nuclear science facility and demonstration power plant with demountable magnets”. en. In: *Fusion Engineering and Design* 100 (Nov. 2015), pp. 378–405. ISSN: 09203796. DOI: 10.1016/j.fusengdes.2015.07.008. URL: <https://linkinghub.elsevier.com/retrieve/pii/S0920379615302337> (visited on 12/02/2025).
- [79] V A Soukhanovskii. “A review of radiative detachment studies in tokamak advanced magnetic divertor configurations”. In: *Plasma Physics and Controlled Fusion* 59.6 (June 2017), p. 064005. ISSN: 0741-3335, 1361-6587. DOI: 10.1088/1361-6587/aa6959. URL: <https://iopscience.iop.org/article/10.1088/1361-6587/aa6959> (visited on 10/24/2025).
- [80] W. M. Stacey and Cheonho Bae. “Representation of the plasma fluid equations in “Miller equilibrium” analytical flux surface geometry”. en. In: *Physics of Plasmas* 16.8 (Aug. 2009), p. 082501. ISSN: 1070-664X, 1089-7674. DOI: 10.1063/1.3177613. URL: <https://pubs.aip.org/pop/article/16/8/082501/316133/Representation-of-the-plasma-fluid-equations-in> (visited on 12/17/2024).
- [81] G. Staebler et al. “Quasilinear theory and modelling of gyrokinetic turbulent transport in tokamaks”. In: *Nuclear Fusion* 64.10 (Oct. 2024), p. 103001. ISSN: 0029-5515, 1741-4326. DOI: 10.1088/1741-4326/ad6ba5. URL: <https://iopscience.iop.org/article/10.1088/1741-4326/ad6ba5> (visited on 05/12/2025).
- [82] G. M. Staebler, J. E. Kinsey, and R. E. Waltz. “A theory-based transport model with comprehensive physics”. en. In: *Physics of Plasmas* 14.5 (May 2007), p. 055909. ISSN: 1070-664X, 1089-7674. DOI: 10.1063/1.2436852. URL: <https://pubs.aip.org/pop/article/14/5/055909/929642/A-theory-based-transport-model-with-comprehensive> (visited on 10/24/2025).
- [83] G.M. Staebler et al. “Verification of a quasi-linear model for gyrokinetic turbulent transport”. en. In: *Nuclear Fusion* 61.11 (Nov. 2021), p. 116007. ISSN: 0029-5515, 1741-4326. DOI: 10.1088/1741-4326/ac243a. URL: <https://iopscience.iop.org/article/10.1088/1741-4326/ac243a> (visited on 02/15/2022).

- [84] Iter Physics Expert Group On Confin Transport, Iter Physics Expert Group On Confin Database, and Iter Physics Basis Editors. “Chapter 2: Plasma confinement and transport”. In: *Nuclear Fusion* 39.12 (Dec. 1999), pp. 2175–2249. ISSN: 0029-5515. DOI: 10.1088/0029-5515/39/12/302. URL: <https://iopscience.iop.org/article/10.1088/0029-5515/39/12/302> (visited on 12/02/2025).
- [85] N. A. Uckan and ITER Physics Group. “ITER Physics Design Guidelines”. en. In: *Fusion Technology* 19.3P2B (May 1991), pp. 1493–1498. ISSN: 0748-1896. DOI: 10.13182/FST19-1493. URL: <https://www.tandfonline.com/doi/full/10.13182/FST19-1493> (visited on 10/29/2025).
- [86] D Van Eester et al. “Minority and mode conversion heating in (^3He)–H JET plasmas”. In: *Plasma Physics and Controlled Fusion* 54.7 (July 2012), p. 074009. ISSN: 0741-3335, 1361-6587. DOI: 10.1088/0741-3335/54/7/074009. URL: <https://iopscience.iop.org/article/10.1088/0741-3335/54/7/074009> (visited on 11/19/2024).
- [87] R. E. Waltz, R. L. Dewar, and X. Garbet. “Theory and simulation of rotational shear stabilization of turbulence”. en. In: *Physics of Plasmas* 5.5 (May 1998), pp. 1784–1792. ISSN: 1070-664X, 1089-7674. DOI: 10.1063/1.872847. URL: <https://pubs.aip.org/pop/article/5/5/1784/1069037/Theory-and-simulation-of-rotational-shear> (visited on 10/28/2025).
- [88] Jan Weiland. *Collective modes in inhomogeneous plasma: kinetic and advanced fluid theory*. eng. Plasma physics series. Bristol: Inst. of Physics Publ, 2000. ISBN: 9780750305891.
- [89] C F B Zimmermann et al. “Analysis and modelling of momentum transport based on NBI modulation experiments at ASDEX Upgrade”. In: *Plasma Physics and Controlled Fusion* 64.5 (May 2022), p. 055020. ISSN: 0741-3335, 1361-6587. DOI: 10.1088/1361-6587/ac5ae8. URL: <https://iopscience.iop.org/article/10.1088/1361-6587/ac5ae8> (visited on 10/28/2025).
- [90] C. F. B. Zimmermann et al. “Experimental validation of momentum transport theory in the core of H-mode plasmas in the ASDEX Upgrade tokamak”. en. In: *Physics of Plasmas* 31.4 (Apr. 2024), p. 042306. ISSN: 1070-664X, 1089-7674. DOI: 10.1063/5.0203092. URL: <https://pubs.aip.org/pop/article/31/4/042306/3284584/Experimental-validation-of-momentum-transport> (visited on 10/28/2025).